Article

Immunity

Regulatory T Cell-Derived TGF-β1 Controls Multiple Checkpoints Governing Allergy and Autoimmunity

Graphical Abstract

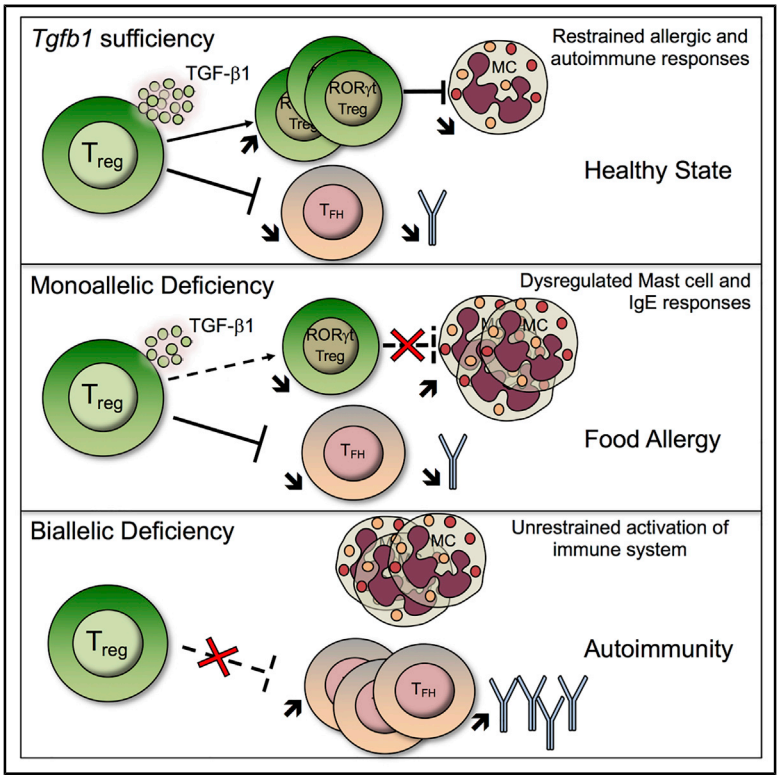

Authors

Jacob A. Turner, Emmanuel Stephen-Victor, Sen Wang, ..., Rima Rachid, Peter T. Sage, Talal A. Chatila

Correspondence

talal.chatila@childrens.harvard.edu

In Brief

The cytokine TGFβ-1 is implicated in controlling allergic and autoimmune responses; however, the specific role of regulatory T (Treg) cell-derived TGF-β1 in governing these responses has been unclear. Turner et al. demonstrate that Treg cell-derived TGF-β1 is critical for restraining allergic and autoimmune diseases in a gene dose-dependent manner.

Highlights

- Treg cell-derived TGF-β1 regulates mast cell and IgE responses
- Treg cell-derived TGF-β1 drives the differentiation of ROR-γt^{+} Treg cells during weaning
- Haploinsufficiency of *Tgfb1* in Treg cells dysregulates the allergic response
- Biallelic deletion of *Tgfb1* in Treg cells precipitates lethal autoimmunity

Turner et al., 2020, Immunity *53*, 1202–1214
December 15, 2020
https://doi.org/10.1016/j.immuni.2020.10.002

CellPress

CellPress

Immunity

Article

Regulatory T Cell-Derived TGF-β1 Controls Multiple Checkpoints Governing Allergy and Autoimmunity

Jacob A. Turner,[1,2,9] Emmanuel Stephen-Victor,[1,2,9] Sen Wang,[1,2] Magali Noval Rivas,[3] Azza Abdel-Gadir,[1,2] Hani Harb,[1,2] Ye Cui,[1,2] Manoussa Fanny,[1,2] Louis-Marie Charbonnier,[1,2] Jason Jun Hung Fong,[1,2] Mehdi Benamar,[1,2] Leighanne Wang,[1,2] Oliver T. Burton,[4] Kushagra Bansal,[5] Lynn Bry,[6] Chengsong Zhu,[7] Quan-Zhen Li,[7] Rachel L. Clement,[8] Hans C. Oettgen,[1,2] Elena Crestani,[1,2] Rima Rachid,[1,2] Peter T. Sage,[8] and Talal A. Chatila[1,2,10,*]

[1]Division of Immunology, Boston Children's Hospital, Boston, MA 02115, USA
[2]Department of Pediatrics, Harvard Medical School, Boston, MA 02115, USA
[3]Division of Pediatric Infectious Diseases and Immunology, Department of Biomedical Sciences, Infectious and Immunologic Diseases Research Center (IIDRC), Cedars-Sinai Medical Center, Los Angeles, CA 90048, USA
[4]Laboratory of Lymphocyte Signaling and Development, The Babraham Institute, Cambridgeshire CB22 3AT, UK
[5]Molecular Biology & Genetics Unit, Jawaharlal Nehru Centre for Advanced Scientific Research, Jakkur, Bangalore 560064, India
[6]Massachusetts Host-Microbiome Center, Department of Pathology, Brigham & Women's Hospital, Harvard Medical School, Boston, MA 02115, USA
[7]Department of Immunology and Internal Medicine, University of Texas Southwestern Medical Center, Dallas, TX 75390, USA
[8]Transplantation Research Center, Renal Division, Brigham and Women's Hospital, Harvard Medical School, Boston, MA 02115, USA
[9]These authors contributed equally
[10]Lead Contact
*Correspondence: talal.chatila@childrens.harvard.edu
https://doi.org/10.1016/j.immuni.2020.10.002

SUMMARY

The mechanisms by which regulatory T (Treg) cells differentially control allergic and autoimmune responses remain unclear. We show that Treg cells in food allergy (FA) had decreased expression of transforming growth factor beta 1 (TGF-β1) because of interleukin-4 (IL-4)- and signal transducer and activator of transcription-6 (STAT6)-dependent inhibition of *Tgfb1* transcription. These changes were modeled by Treg cell-specific *Tgfb1* monoallelic inactivation, which induced allergic dysregulation by impairing microbiota-dependent retinoic acid receptor-related orphan receptor gamma t (ROR-γt)$^+$ Treg cell differentiation. This dysregulation was rescued by treatment with Clostridiales species, which upregulated *Tgfb1* expression in Treg cells. Biallelic deficiency precipitated fatal autoimmunity with intense autoantibody production and dysregulated T follicular helper and B cell responses. These results identify a privileged role of Treg cell-derived TGF-β1 in regulating allergy and autoimmunity at distinct checkpoints in a *Tgfb1* gene dose- and microbiota-dependent manner.

INTRODUCTION

The incidence of immune dysregulatory diseases, including allergic and autoimmune diseases, has increased in recent decades, reflecting altered environmental influences (Bach, 2002, 2018; Platts-Mills, 2015). A key mechanism by which these diseases develop involves perturbation of immune tolerance mediated by regulatory T (Treg) cells (Grant et al., 2015; Noval Rivas and Chatila, 2016). Of the several mechanisms implicated in Treg cell-mediated enforcement of peripheral immune tolerance, the role of Treg cell-derived transforming growth factor beta (TGF-β) remains enigmatic, given the broad expression of TGF-β species among different immune and non-immune cells (Travis and Sheppard, 2014). In particular, although TGF-β has been implicated in immunosuppression by Treg cells (Cuende et al., 2015; Li et al., 2007; Marie et al., 2005), other studies have indicated that Treg cell-derived TGF-β1, the major TGF-β species expressed by T cells, is largely redundant in immune regulation (Edwards et al., 2016; Gutcher et al., 2011). In this study, we demonstrate that, despite being abundantly available from other cell sources, TGF-β1 derived from Treg cells fulfils non-redundant functions in controlling allergic and autoimmune responses by distinct mechanisms segregated by Treg cell *Tgfb1* gene dose and microbiota dependency.

RESULTS

T Helper 2 (Th2) Cell-like Reprogramming of Treg Cells Promotes Allergic Dysregulation by Suppressing *Tgfb1* Transcription

Oral tolerance is dependent on differentiation of Foxp3$^+$Helios$^-$ induced Treg (iTreg) cells from naive CD4$^+$Foxp3$^-$ T cells (CD4$^+$ Teff cells) upon their activation by antigen-presenting CD103$^+$ dendritic cells (DCs) in the presence of TGF-β1 (Apostolou and

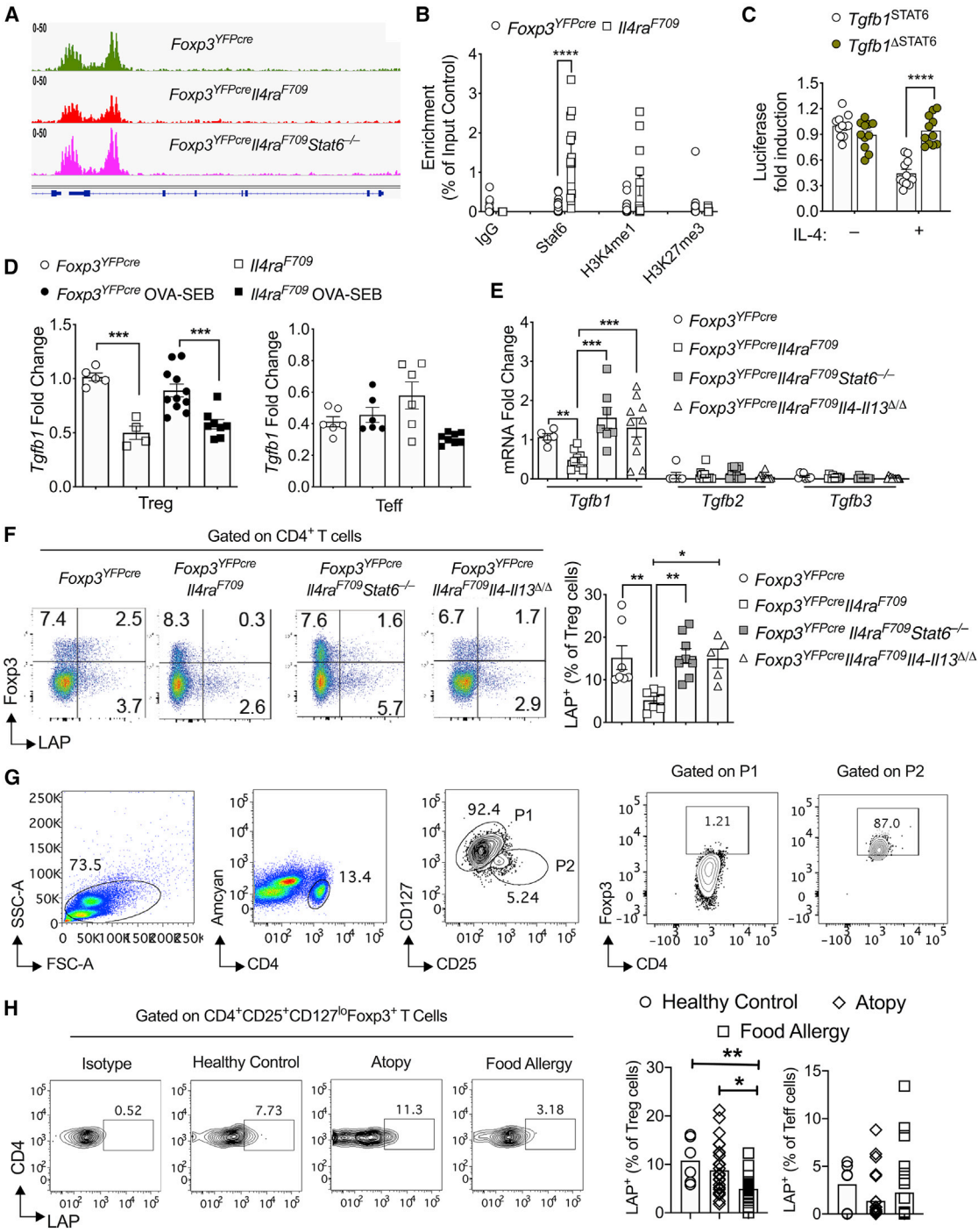

Figure 1. Suppression of *Tgfb1* Expression by IL-4R Signaling in Treg Cells

(A) ATAC-seq analysis of the *Tgfb1* locus in Treg cells of the respective genotypes.

(B) ChIP assays for binding of STAT6, H3K4me1, H3K27me3, and control (IgG) antibodies to the *Tgfb1* promoter in Treg cells of *Foxp3*^{YFPcre} mice.

(C) Luciferase reporter assays for *Tgfb1* promoters with or without the STAT6 binding site, treated as indicated.

(D) RT-PCR of *Tgfb1* transcripts in splenic Treg and Teff cells sorted from *Foxp3*^{YFPcre} and *Foxp3*^{YFPcre}*Il4ra*^{F709} sham and OVA-SEB-sensitized mice. Transcript expression in CD4$^+$ Teff cells is also shown.

(E) *Tgfb1-3* transcripts in *Foxp3*^{YFPcre}, *Foxp3*^{YFPcre}*Il4ra*^{F709}, *Foxp3*^{YFPcre}*Il4ra*^{F709} *Il4-Il13*$^{\Delta/\Delta}$, and *Foxp3*^{YFPcre}*Il4ra*^{F709}*Stat6*$^{-/-}$ splenic Treg cells, with the latter sufficient or deficient in *Il4-Il13* or *Stat6*.

(F) Flow cytometry analysis and frequencies of LAP$^+$ staining in Treg cells sorted from the respective mouse strains.

(G) Flow cytometry (fluorescence-activated cell sorting [FACS]) plots showing the gating strategy for human Treg and Teff cells.

(H) LAP staining on Treg cells isolated from peripheral blood mononuclear cells (PBMCs) of FA, atopics without FA, and healthy subjects.

(legend continued on next page)

von Boehmer, 2004; Esterházy et al., 2016; Haribhai et al., 2009; Mucida et al., 2005). With food allergy (FA), allergen-specific Treg cells undergo Th2 cell-like reprogramming, which disables their regulatory function and promotes disease (Noval Rivas et al., 2015). Interruption of this process by deletion of *Stat6* or Treg cell-specific *Il4* and *Il13* restores Treg cell regulation and suppresses FA (Abdel-Gadir et al., 2018; Noval Rivas et al., 2015). We employed FA-prone mice that carry a gain-of-function mutation in the interleukin-4Rα IL-4Rα) chain gene ($Il4ra^{F709}$) to investigate the mechanisms by which FA develops in these mice (Noval Rivas et al., 2015; Tachdjian et al., 2010). Epigenetic analysis of mesenteric lymph node Treg cells isolated from $Il4ra^{F709}$ mice using an assay for transposase-accessible chromatin sequencing (ATAC-seq) revealed decreased access at the *Tgfb1* locus that was reversed by deletion of *Stat6* (Figure 1A). Chromatin immunoprecipitation (ChIP) studies demonstrated increased binding of STAT6 to the *Tgfb1* promoter of $Il4ra^{F709}$ Treg cells in association with increased H3K4me1 but not H3K27me3, a histone marker configuration indicative of an active enhancer state (Figure 1B; Heintzman et al., 2007).

Consistent with a transcriptional suppression mechanism of the *Tgfb1* promoter by STAT6, luciferase reporter assays revealed that treatment with IL-4 decreased *Tgfb1* promoter activity by about 50% and that inactivation of a candidate STAT6 binding element within the promoter reversed that inhibition (Figure 1C). In agreement with these findings, expression of *Tgfb1* transcripts was decreased by 50% in Treg but not Teff cells of $Il4ra^{F709}$ mice compared with *Il4ra* wild-type mice. This decrease was normalized upon deletion of *Stat6* or Treg cell-specific deletion of *Il4 and Il13* using a yellow fluorescent protein (YFP)-Cre recombinase fusion protein encoded by the endogenous *Foxp3* locus ($Foxp3^{YFPcre}$) (Figures 1D and 1E; Rubtsov et al., 2008). In contrast, there was minimal expression of *Tgfb2* and *Tgfb3* in Treg cells, which was not affected by *Stat6* or *Il4* and *Il13* deletion (Figure 1E). Expression of the TGF-β1 precursor latency-associated protein (LAP) was also decreased in Treg cells of $Il4ra^{F709}$ mice compared with control mice but normalized upon deletion of *Il4-Il13* or *Stat6* (Figure 1F). Importantly, subjects with FA, whose circulating Treg cells ($CD4^+CD25^+CD127^{lo}FOXP3^+$; see gating strategy in Figure 1G) exhibit Th2 cell-like reprograming (Noval Rivas et al., 2015), had decreased LAP staining of their Treg cells compared with non-FA atopic or non-atopic controls (Figures 1G and 1H; see Table S1 for subject demographics). Overall, these results established that FA-promoting Th2 cell-like reprogramming of Treg cells is associated with decreased LAP expression in mice and human subjects with FA.

A direct role of decreased *Tgfb1* expression in Treg cells in promoting FA was corroborated by overexpressing a $Foxp3^{YFPcre}$-regulated *Tgfb1* transgene ($Tgfb1^{Tg}$) in Treg cells of $Il4ra^{F709}$ mice (Hall et al., 2010). Analysis of $Il4ra^{F709}Foxp3^{YFPcre}Tgfb1^{Tg}$ mice revealed that *Tgfb1* Tg expression upregulated *Tgfb1* transcripts and LAP surface expression in $Il4ra^{F709}$ Treg cells but not in $CD4^+$ Teff cells (Figure S1). Although oral sensitization of $Il4ra^{F709}$ mice with chicken egg ovalbumin (OVA) mixed with the mucosal adjuvant staphylococcal enterotoxin B (OVA/SEB) followed by oral challenge with OVA resulted in profound anaphylaxis, $Il4ra^{F709}Foxp3^{YFPcre}Tgfb1^{Tg}$ mice were completely protected. $Tgfb1^{Tg}$ expression in Treg cells of $Il4ra^{F709}$ mice completely suppressed the elevation in total and OVA-specific immunoglobulin E (IgE) antibodies induced by oral allergic sensitization. It also suppressed mast cell degranulation following oral challenge with OVA and the $CD4^+$ Teff Th2 cell response (Figure S1). These results indicated that the Th2 cell-like reprogramming in Treg cells suppresses *Tgfb1* transcription to promote FA.

Treg Cell-specific *Tgfb1* Haploinsufficiency Promotes Allergic Dysregulation

To further determine the role of decreased Treg cell-derived TGF-β1 in mediating FA, we employed mice heterozygous for a single floxed *Tgfb1* allele crossed with $Foxp3^{YFPcre}$ (Figure 2A). Oral sensitization of $Foxp3^{YFPcre}Tgfb1^{\Delta/+}$ mice, but not $Foxp3^{YFPcre}$ mice, with OVA/SEB followed by oral challenge with OVA resulted in anaphylaxis, as monitored by a drop in core body temperature. Total serum IgE concentrations were elevated in $Foxp3^{YFPcre}Tgfb1^{\Delta/+}$ mice at baseline, and OVA-specific IgE responses rose sharply post-sensitization, indicative of allergic dysregulation (Figure 2B). Mast cell degranulation, as evidenced by increased serum mouse mast cell protease-1 (MMCP-1), was increased in sensitized $Foxp3^{YFPcre}Tgfb1^{\Delta/+}$ mice following oral challenge with OVA, in association with exaggerated gut tissue mastocytosis, impaired differentiation of iTreg cells, and increased Th2 cell responses (Figures 2B–2G).

Retinoic acid receptor-related orphan receptor gamma t $(ROR\text{-}\gamma t)^+$ iTreg cells differentiate under the influence of microbial signals and have a critical role in suppressing Th2 cell responses, including FA (Abdel-Gadir et al., 2019; Ohnmacht et al., 2015; Sefik et al., 2015). In particular, a bloom in Clostridiales and Bacteroidales species at the time of weaning sets a critical timed window for differentiation of a durable $ROR\text{-}\gamma t^+$ iTreg cell population that suppresses aberrant gut pathologies (Al Nabhani et al., 2019; Stephen-Victor et al., 2020). Analysis of small intestinal *lamina propria* lymphocytes (SI-LPLs) following weaning (day 28) revealed decreased frequencies of $ROR\text{-}\gamma t^+$ Treg cells in $Foxp3^{YFPcre}Tgfb1^{\Delta/+}$ mice to become similar to those seen in $Il4ra^{F709}$ mice (Abdel-Gadir et al., 2019). In contrast, biallelic *Tgfb1* inactivation in Treg cells of $Foxp3^{YFPcre}Tgfb1^{\Delta/\Delta}$ mice abrogated $ROR\text{-}\gamma t^+$ Treg cell differentiation (Figure 3A). In contrast, $GATA\text{-}3^+$ Treg cells were reciprocally increased. Consistent with these results, $ROR\text{-}\gamma t^+$ Treg cells were enriched in the LAP^+ Treg cell population in the SI-LP of microbiota-sufficient specific pathogen-free (SPF) mice (Figure 3B). Furthermore, gut Treg cells of germ-free (GF) mice, which are lacking in the microbiota-dependent $ROR\text{-}\gamma t^+$ subpopulation, also exhibited decreased LAP staining and *Tgfb1* mRNA expression compared with SPF mice (Figures 3C and 3D). Reconstitution of GF mice with a consortium of immunomodulating Clostridiales species, but not one composed of Proteobacteria species (Abdel-Gadir et al., 2019),

Each symbol represents an independent sample. Numbers in flow plots indicate percentages. Error bars indicate SEM. Statistical tests: Student's t test (B), two-way ANOVA (C), and one-way ANOVA with Dunnett's post hoc analysis (D–G). *p < 0.05, **p < 0.01, ***p < 0.001, ****p < 0.0001. Data are representative of two or three independent experiments. n = 5–13 mice per group (B), 11 replicates per group (C), 4–14 mice per group (D–F), and 6–26 subjects (G). See also Figure S1.

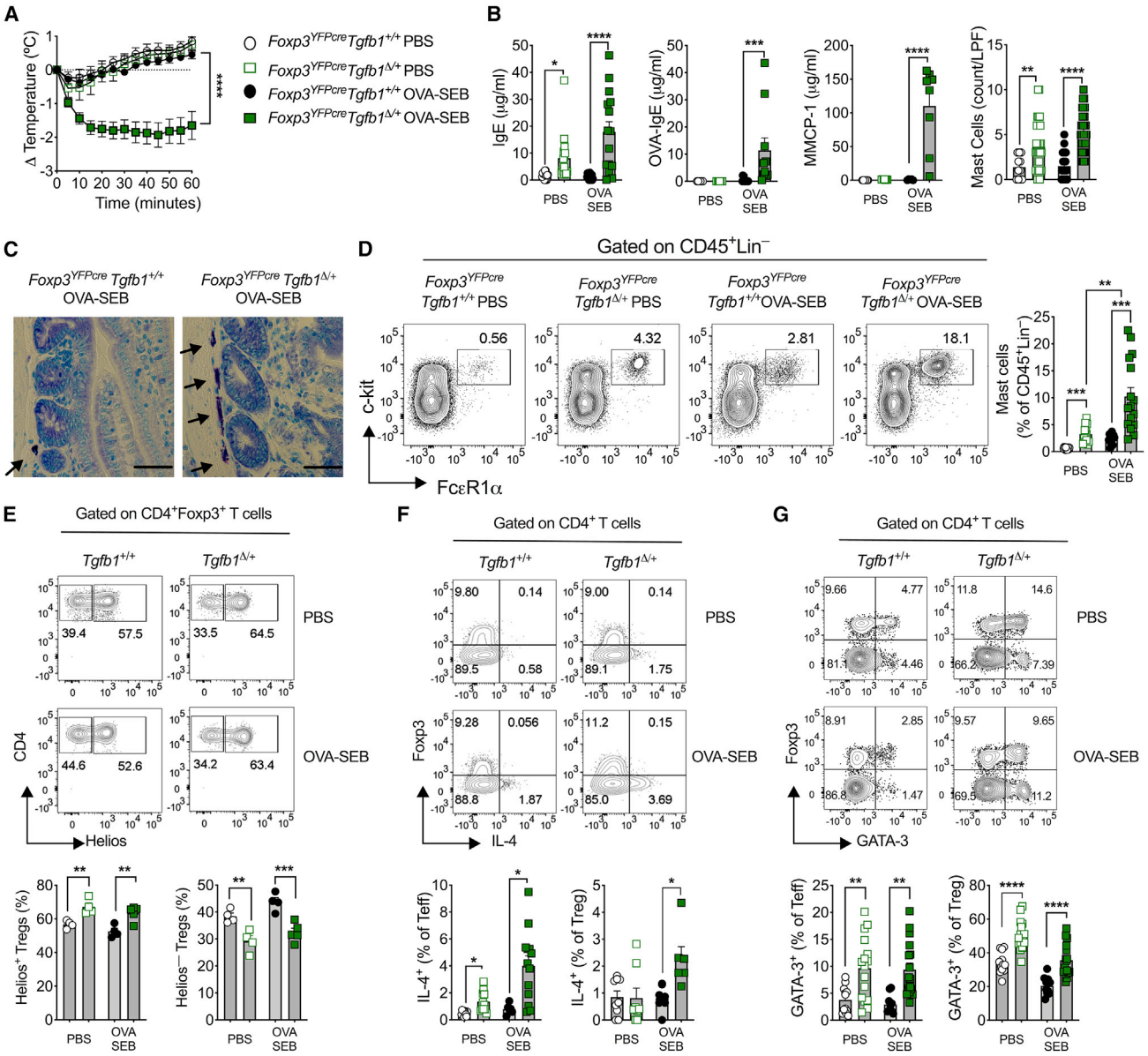

Figure 2. Treg Cell-Specific *Tgfb1* Haploinsufficiency Promotes Allergic Dysregulation

(A) Core body temperature drop following OVA challenge of OVA/SEB-sensitized wild-type (WT), *Il4ra*^{F709}, and *Foxp3*^{YFPcre}*Tgfb1*$^{\Delta/+}$ mice.

(B) Serum total and OVA-specific IgE and MMCP-1 mast cell counts from the histology of the SI.

(C) Microscopy pictures (original magnification, ×600) of toluidine blue-stained histological sections from the jejunum of mice sensitized and challenged in (A). Arrows indicate mast cells.

(D) Flow cytometry analysis of mast cells in SI-LPLs of mice challenged in (A).

(E–G) Flow cytometry analysis and frequencies of Helios$^+$ and Helios$^-$ Treg cells (E) and IL-4$^+$ (F) and GATA-3$^+$ (G) Treg and Teff cells among SI-LPLs of mice from (A).

Each symbol represents an independent sample. Numbers in flow plots indicate percentages. Error bars indicate SEM. Statistical tests: repeated-measures two-way ANOVA (A) and one-way ANOVA with Dunnett's post hoc analysis (B, E, and F). *p < 0.05, **p < 0.01, ***p < 0.001, ****p < 0.0001. Data are representative of at least three independent experiments with 9–31 mice per group (A) and 5–17 mice per group (B and E–G).

upregulated ROR-γt, LAP, and *Tgfb1* expression in gut Treg cells to become similar to those seen in Treg cells of SPF mice (Figures 3C and 3D). These results indicate that immunomodulatory commensal bacteria upregulate *Tgfb1* expression in gut Treg cells, a necessary step in promoting their differentiation into ROR-γt$^+$ Treg cells.

Given that immunomodulating Clostridiales species suppress FA by inducing ROR-γt$^+$ Treg cells (Abdel-Gadir et al., 2019), we examined the capacity of treatment with the Clostridiales consortium to rescue allergic dysregulation in *Foxp3*^{YFPcre}*Tgfb1*$^{\Delta/+}$ mice. Treatment with the Clostridiales consortium suppressed anaphylaxis in OVA/SEB-sensitized and OVA-challenged

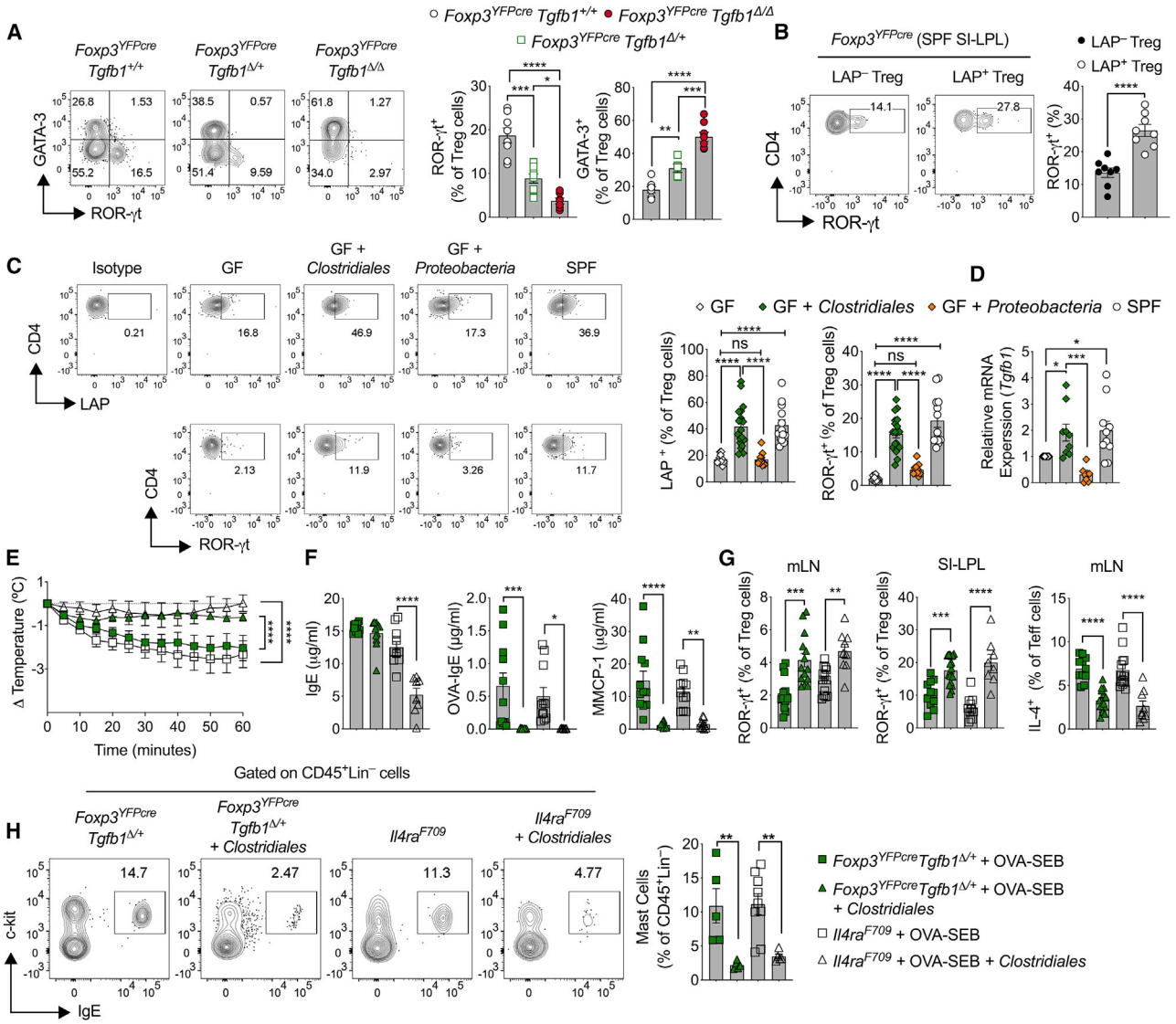

Figure 3. Treg Cell-Derived TGF-β1 Enables Oral Tolerance by Promoting ROR-γt+ Gut Treg Cell Differentiation

(A) Flow cytometry analysis and cell frequencies of ROR-γt and GATA3 staining in SI-LPL Treg cells isolated from 4-week-old *Foxp3*^{YFPcre}, *Foxp3*^{YFPcre}*Tgfb1*$^{\Delta/+}$, and *Foxp3*^{YFPcre}*Tgfb1*$^{\Delta/\Delta}$ mice.

(B) Flow cytometry analysis and cell frequencies of ROR-γt expression in LAP$^+$ and LAP$^-$ SI-LPL Treg cells.

(C) Flow cytometry analysis and cell frequencies of LAP and ROR-γt expression in SI-LPL Treg cells of GF mice, GF mice reconstituted with Clostridiales or Proteobacteria consortia, and SPF mice.

(D) RT-PCR analysis of *Tgfb1* mRNA expression in the mouse groups in (C).

(E) Temperature changes in OVA/SEB-sensitized *Foxp3*^{YFPcre}*Tgfb1*$^{\Delta/+}$ and *Il4ra*^{F709} mice that were left untreated or treated with Clostridiales during sensitization and then challenged with OVA.

(F) Serum total and OVA-specific IgE and serum MMCP-1.

(G) Frequencies of ROR-γt$^+$ Treg cells in MLNs and SI-LPLs and of IL-4$^+$ Treg cells in MLNs of the mouse groups in (E).

(H) Flow cytometry analysis of SI c-Kit$^+$FcεRI$^+$ mast cells and their frequencies in the mouse groups in (E).

Each symbol represents an independent sample. Numbers in flow plots indicate percentages. Error bars indicate SEM. Statistical tests: one-way ANOVA with Dunnett's post hoc analysis (A–D and F–H) and repeated-measures two-way ANOVA (E); *p < 0.05, **p < 0.01, ***p < 0.001, ****p < 0.0001. Data are representative of at least three independent experiments with 5–8 mice per group (A and B) and 4–19 mice (C and E–H).

Foxp3^{YFPcre}*Tgfb1*$^{\Delta/+}$ mice in a manner similar to that seen in similarly sensitized and challenged Clostridiales-treated *Il4ra*^{F709} mice, in association with profoundly decreased OVA-specific IgE and MMCP-1 release (Figures 3E and 3F; Abdel-Gadir et al., 2019). Microbial therapy with the Clostridiales consortium upregulated induction of ROR-γt$^+$ Treg cells and suppressed IL-4 production by T cells and mast cell expansion in the mesenteric lymph nodes (MLNs) and SI-LPLs of both mouse strains (Figures 3G and 3H). These results are consistent with a critical role of Treg cell-derived TGF-β1 in mediating

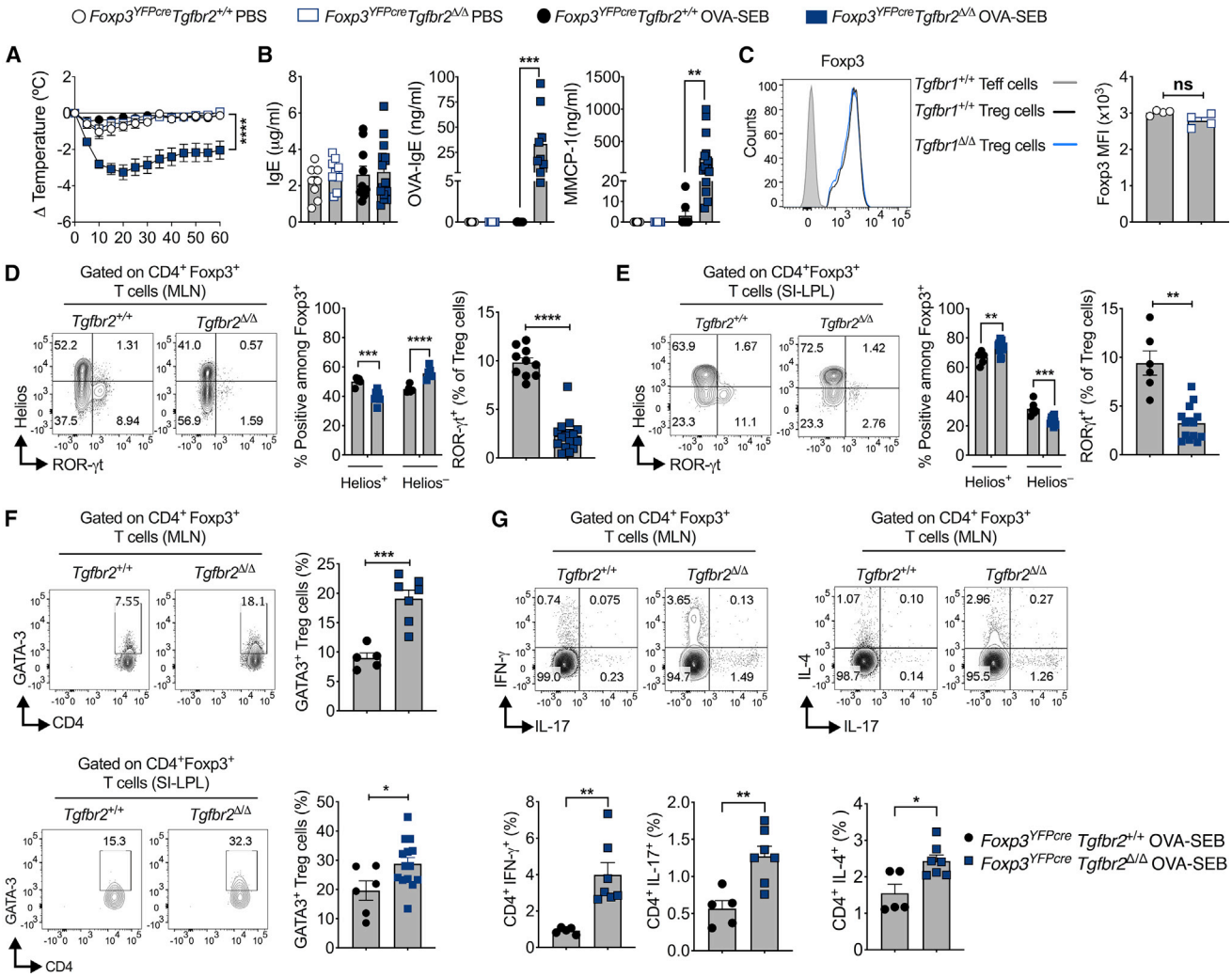

Figure 4. Treg Cell-Specific *Tgfbr2* Deficiency Impairs Oral Tolerance

(A) Core body temperature drop following OVA challenge of OVA-SEB sensitized WT and *Foxp3*^{YFPcre}*Tgfbr2*$^{\Delta/\Delta}$ mice.

(B) Serum concentrations of IgE, OVA-specific IgE, and MMCP-1.

(C) Flow cytometry analysis of the mean fluorescence intensity (MFI) of Foxp3 in Treg cells isolated from MLNs.

(D and E) Flow cytometry analysis and frequencies of Helios$^+$, Helios$^-$, and ROR-γt$^+$ cells among CD4$^+$Foxp3$^+$ Treg cells from MLNs (D) and SI-LPLs (E) of mice from (A).

(F) Flow cytometry analysis and frequencies of GATA3$^+$ cells among CD4$^+$Foxp3$^+$ Treg cells from MLNs and SI-LPLs of mice from (A).

(G) Flow cytometry analysis and frequencies of Teff cytokines.

Each symbol represents an independent sample. Numbers in flow plots indicate percentages. Error bars indicate SEM. Statistical tests: two-way ANOVA (A, D, and E) and Student's t test (B–G). *p < 0.05, **p < 0.01, ***p < 0.001, ****p < 0.0001. Data are representative of two independent experiments. n = 4–16 mice per group.

microbiota-dependent oral tolerance by promoting ROR-γt$^+$ Treg cell differentiation.

The contribution of Treg cell-intrinsic TGF-β1 signaling to the allergic response was addressed by means of Treg cell-specific deletion of *Tgfbr2*, encoding TGF-β receptor subunit II (TGF-βR2). As documented previously, these mice are generally healthy (Konkel et al., 2017; Wu et al., 2017). Oral sensitization of *Foxp3*^{YFPcre}*Tgfbr2*$^{\Delta/\Delta}$ mice with OVA/SEB rendered the mice susceptible to robust anaphylaxis upon oral challenge with OVA (Figures 4A and 4B). Notably, *Foxp3*^{YFPcre}*Tgfbr2*$^{\Delta/\Delta}$ mice exhibited increased iTreg cells (Foxp3$^+$Helios$^-$) in the MLNs, whereas differentiation of iTreg cells in SI-LPLs was impaired in allergen-sensitized mice (Figures 4D and 4E). Critically, differentiation of ROR-γt$^+$ Treg cells was profoundly suppressed in the MLNs and SI-LP of allergen-sensitized *Foxp3*^{YFPcre}*Tgfbr2*$^{\Delta/\Delta}$ mice. Reciprocally, expansion of GATA3$^+$ Treg cells was increased in *Foxp3*^{YFPcre}*Tgfbr2*$^{\Delta/\Delta}$ mice and was associated with heightened T helper cell responses (Figures 4D–4F). Overall, these findings indicated a requisite role of TGF-β1 signaling in nascent gut Treg cells for differentiation of ROR-γt$^+$ Treg cells and in controlling FA.

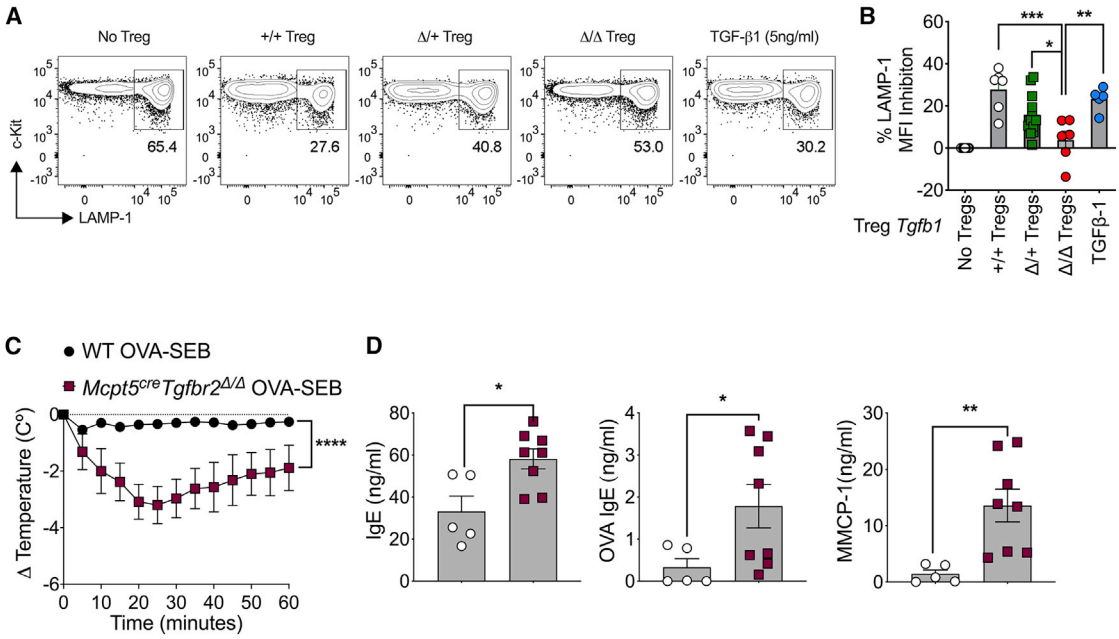

Figure 5. TGF-β1-Deficient Treg Cells Fail to Suppress Mast Cell Degranulation

(A and B) Flow cytometry analysis of LAMP1 staining (A) and quantification of percent LAMP1 MFI inhibition (B) from *in vitro* bone marrow mast cell suppression assay with sorted MLN Treg cells from 8-week-old *Foxp3*^{YFPcre} (+/+), *Foxp3*^{YFPcre}*Tgfb1*$^{Δ/+}$ (Δ/+), and *Foxp3*^{EGFPcre}*Tgfb1*$^{Δ/Δ}$ (Δ/Δ) mice or mast cells treated with recombinant TGF-β1 (5 ng/mL).

(C) Core body temperature drop following OVA challenge of OVA-SEB sensitized WT and *Mcpt5*^{cre}*Tgfbr2*$^{Δ/Δ}$ mice.

(D) Serum concentrations of total IgE, OVA-specific IgE, and MMCP-1.

Each symbol represents an independent sample. Numbers in flow plots indicate percentages. Error bars indicate SEM. Statistical tests: one-way ANOVA with Dunnett's post hoc analysis (B), two-way ANOVA (C), and Student's t test (D). *p < 0.05, **p < 0.01, ***p < 0.001, ****p < 0.0001. Data are representative of two independent experiments. n = 6–12 replicates per group (A and B) and 5–8 mice per group (C and D).

Treg Cell-Derived TGF-β1 Restrains Mast Cell Expansion and Activation

The mechanisms by which Treg cell-derived TGF-β1 affected different components of the allergic response was analyzed. Previous studies have invoked a role of TGF-β1 in regulating mast cell activation, leading us to investigate the role of Treg cell-derived TGF-β1 in regulating mast cell functions (Gomez et al., 2005). Treatment of 2,4-dinitrophenyl-bovine serum albumin (DNP-BSA) primed mast cells with IgE resulted in mast cell activation and degranulation, marked by increased surface expression of the granule marker LAMP-1 (CD107a) (Burton et al., 2013; Grützkau et al., 2004; Noval Rivas et al., 2015). Addition of Treg cells derived from MLNs of *Foxp3*^{YFPcre} mice or recombinant TGF-β1 attenuated LAMP-1 induction upon mast cell exposure to antigen, whereas Treg cells derived from MLNs of *Foxp3*^{YFPcre}*Tgfb1*$^{Δ/+}$ and *Foxp3*^{YFPcre}*Tgfb1*$^{Δ/Δ}$ mice failed to do so in a *Tgfb1* gene dose-dependent manner (Figures 5A and 5B). Reciprocally, deletion of a floxed *Tgfbr2* allele in mast cells using a mast cell protease 5 gene promoter-driven Cre recombinase (*Mcpt5*^{cre}) precipitated susceptibility to FA and anaphylaxis (Figures 5C and 5D). Collectively, these results indicate a critical function of Treg cell-derived TGF-β1 signaling in regulating mast cell responses.

Treg Cell-Specific Biallelic *Tgfb1* Deletion Precipitates Intense Autoimmunity

Although partial depletion of *Tgfb1* transcripts effected by Treg cell-specific inactivation of a single *Tgfb1* allele rendered mice highly allergic, their near complete depletion in Treg cells by means of *cre*-mediated deletion of both alleles (*Foxp3*^{YFPcre}*Tgfb1*$^{Δ/Δ}$) in the face of sustained *Tgfb1* expression in Teff cells precipitated a rapidly fatal autoimmune lymphoproliferative disease that was phenotypically similar to that associated with Foxp3 deficiency (Scurfy phenotype) (Figures 6A–6D; Figure S2A; Charbonnier et al., 2019; Lin et al., 2005). Flow cytometry analysis revealed decreased LAP expression on Treg cells of *Foxp3*^{YFPcre}*Tgfb1*$^{Δ/+}$ and *Foxp3*^{YFPcre}*Tgfb1*$^{Δ/Δ}$ as a function of *Tgfb1* allele deficiency (Figure S2B). In contrast, the low expression of LAP on Teff cells in the respective strains was increased marginally (Figure S2C). Notably, Treg cell expression of glycoprotein-A repetition-predominant protein (GARP), which binds to LAP and enables its activation and is itself implicated in regulating allergy and autoimmunity (Liénart et al., 2018; Nasrallah et al., 2020; Tran et al., 2009), was also decreased in a stepwise manner as a function of *Tgfb1* allele deficiency (Figure S2D). Consistent with these results, TGF-β1 production by activated Treg cells was progressively decreased in *Foxp3*^{YFPcre}*Tgfb1*$^{Δ/+}$ and *Foxp3*^{YFPcre}*Tgfb1*$^{Δ/Δ}$ mice as a function Treg cell-specific allele deficiency. In contrast, TGF-β1 production in Teff cells, B cells, and monocytes was increased in *Foxp3*^{YFPcre}*Tgfb1*$^{Δ/Δ}$ in comparison with *Foxp3*^{YFPcre}*Tgfb1*$^{Δ/+}$ and *Foxp3*^{YFPcre}*Tgfb1*$^{Δ/Δ}$ mice (Figures S2E–S2G). Further analysis revealed that expression of LAP in MLN CD11c^{+}MHCII^{+} DCs stimulated with LPS was similar in magnitude in *Foxp3*^{YFPcre} and *Foxp3*^{YFPcre}*Tgfb1*$^{Δ/+}$ mice, whereas LAP expression was enhanced in the equivalent

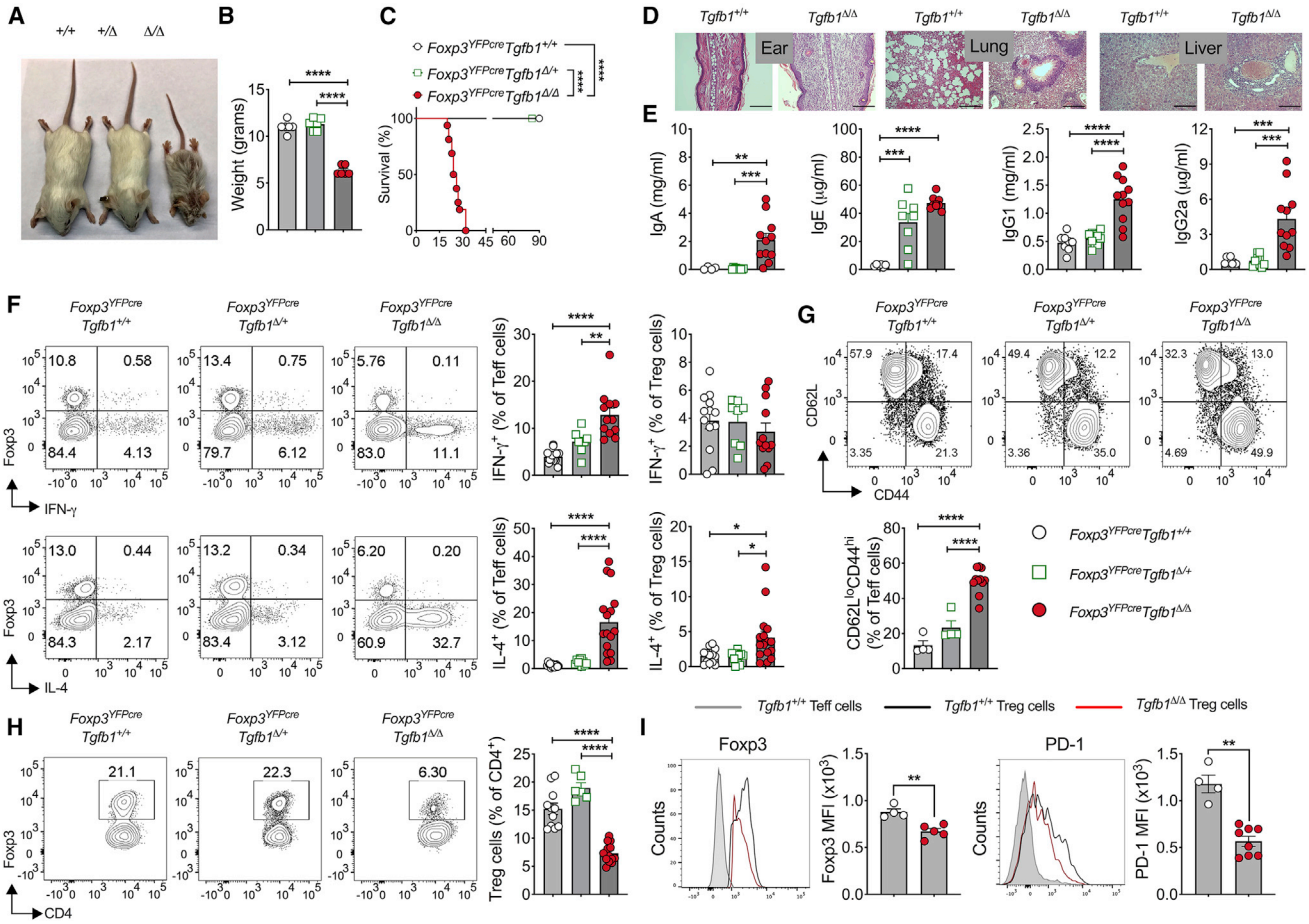

Figure 6. Biallelic Treg Cell *Tgfb1* Deficiency Precipitates Fatal Autoimmunity

(A) Appearance of *Foxp3*^{YFPcre}, *Foxp3*^{YFPcre}*Tgfb1*$^{\Delta/+}$, and *Foxp3*^{YFPcre}*Tgfb1*$^{\Delta/\Delta}$ littermate mice.

(B) Body weights at 19 days of age.

(C) Survival curves of the respective mouse strains.

(D) Histology pictures of skin, lung, and liver tissue stained with hematoxylin and eosin (original magnification, ×200).

(E) Serum immunoglobulin concentrations.

(F) Flow cytometry analysis and cell frequencies of IL-4 and interferon γ (IFNγ) expression in splenic Treg and Teff cells.

(G) Flow cytometry analysis of CD62 and CD44 staining on splenic CD4$^+$ T cells (left) and cell frequencies of CD62^{low}CD44^{high} Teff cells.

(H) Flow cytometry analysis and cell frequencies of CD4$^+$Foxp3$^+$ Treg cells.

(I) Flow cytometry analysis and MFI of Foxp3 and PD-1 expression in splenic Treg cells.

Each symbol represents an independent sample. The age of the mice in (A) and (C)–(H) was between 3 and 4 weeks. Numbers in flow plots indicate percentages. Error bars indicate SEM. Statistical tests: log rank test (A), Student's t test (C and F–J), and one-way ANOVA with Dunnett's post hoc analysis (D). *p < 0.05, **p < 0.01, ***p < 0.001, ****p < 0.0001. Data are representative of 2–3 independent experiments with 4–16 mice per group. See also Figures S2–S6.

DCs from *Foxp3*^{YFPcre}*Tgfb1*$^{\Delta/\Delta}$ mice, likely because of their activation (Figure S3D). *Foxp3*^{YFPcre}*Tgfb1*$^{\Delta/\Delta}$ mice exhibited hypergammaglobulinemia and skewing of their T cells toward an effector memory phenotype compared with *Foxp3*^{YFPcre}*Tgfb1*$^{\Delta/+}$ and *Foxp3*^{YFPcre} littermates (Figures 6E and 6G). There were increased frequencies of IL-4$^+$ and IFN-γ$^+$ Teff cells (Figure 6F), whereas that of IL-17$^+$ Teff cells were unchanged (data not shown). The frequencies of peripheral Treg cells was decreased in *Foxp3*^{YFPcre}*Tgfb1*$^{\Delta/\Delta}$ mice in association with decreased expression of certain markers, including Foxp3, PD-1, and NRP-1 in the face of normal or increased expression of others, including CD25, CTLA4, OX40, and ICOS, and normal expression of the proliferation marker Ki-67 (Figures 6H and 6I; Figures S3A and S3B). IL-10 expression was similar in MLN Treg cells of *Foxp3*^{YFPcre} and *Foxp3*^{YFPcre}*Tgfb1*$^{\Delta/+}$ mice, whereas it was decreased in *Foxp3*^{YFPcre}*Tgfb1*$^{\Delta/\Delta}$ mice (Figure S3C). *In vitro*, the suppressive capacity of *Foxp3*^{YFPcre}*Tgfb1*$^{\Delta/\Delta}$ Treg cells was decreased compared with *Foxp3*^{YFPcre} Treg cells, whereas that of *Foxp3*^{YFPcre}*Tgfb1*$^{\Delta/+}$ Treg cells was unchanged (Figure S3E). Development of TGF-β1-deficient Treg cells *in vivo* was not altered in healthy *Foxp3*$^{YFPcre/+}$ females homozygous for the *Tgfb1* floxed allele (*Foxp3*$^{YFPcre/+}$*Tgfb1*$^{\Delta/\Delta}$) which, because of the phenomenon of X-linked inactivation, harbor TGF-β1-sufficient and -deficient cells (Figure S3F).

The role of Treg cell *Tgfb1* in regulating allergic and autoimmune responses in a gene dose-dependent manner was further

highlighted in experiments using a bacterial artificial chromosome Tg that enabled expression of a Cre recombinase and enhanced green fluorescent protein (EGFP) in Foxp3$^+$ T cells (*Foxp3*^{EGFPcre}). Unlike *Foxp3*^{YFPcre}*Tgfb1*$^{Δ/Δ}$ mice, bacterial artificial chromosome (BAC) *Foxp3*^{EGFPcre}*Tgfb1*$^{Δ/Δ}$ mice did not suffer lymphoproliferation, and their survival was similar to control mice. Lineage tracing analysis using a *cre*-regulated *Rosa26*-YFP reporter (*Rosa26*^{YFP}) revealed that the majority of Treg cells in *Foxp3*^{EGFPcre}*Tgfb1*$^{Δ/Δ}$*Rosa26*^{YFP} mice did not express *Foxp3* BAC-driven EGFP-Cre Tg (Foxp3$^+$EGFP$^-$YFP$^-$). Accumulation of EGFP$^-$ Treg cells reached up to 60% of the peripheral Treg cell pool (Figures S4A and S4B). We further analyzed the expression of LAP and GARP in Cre-expressing Treg cells (EGFP$^+$Foxp3$^+$), escaped Treg cells (EGFP$^-$Foxp3$^+$) and Teff cells (EGFP$^-$Foxp3$^-$) of *Foxp3*^{EGFPcre}*Tgfb1*$^{Δ/Δ}$ mice. Results revealed that, although the escaped Treg cells exhibited increased expression of LAP and GARP, expression of those proteins was decreased substantially in BAC-expressing Treg cells, reflecting effective deletion of *Tgfb1* in those cells. In contrast, LAP and GARP expression was negligible in Teff cells (Figures S4B and S4C). Of note, oral sensitization of *Foxp3*^{EGFPcre}*Tgfb1*$^{Δ/Δ}$ but not *Foxp3*^{EGFPcre} mice rendered them susceptible to robust anaphylaxis upon oral challenge with OVA (Figure S5A**)**. The OVA FA response of *Foxp3*^{EGFPcre}*Tgfb1*$^{Δ/Δ}$ mice mirrored that observed in similarly treated *Il4ra*^{F709} mice, showing increased total and OVA-specific IgE and elevated serum concentrations of MMCP-1 following anaphylaxis, with SI tissue mast cell expansion (Figures S5B–S5D). MLN Treg cells were increased in OVA FA *Foxp3*^{EGFPcre}*Tgfb1*$^{Δ/Δ}$ mice, indicating that the propensity of these mice to develop FA was not due to a relative deficiency in Treg cells (Figures S5E and S5F). Rather, transfer experiments with TGF-β1-sufficient and deficient *Foxp3*^{EGFPcre} Treg cells bearing the OVA$_{323-339}$ peptide-specific DO11.10 transgenic T cell receptor revealed the capacity of the former but not the latter cells to prevent induction of FA in *Il4ra*^{F709} mice and to suppress existing disease, indicating that it was the relative deficiency of *Tgfb1*-expressing Treg cells that rendered *Foxp3*^{EGFPcre}*Tgfb1*$^{Δ/Δ}$ mice susceptible to FA (Figure S6). Overall, development of an allergic response and transition to a fulminant autoimmune phenotype are regulated by the availability of Treg cell-derived TGF-β1 in a cell frequency- and gene dose-dependent manner.

Treg Cell-Specific Biallelic *Tgfb1* Deletion Dysregulates T Follicular Helper (Tfh) Cell and B Cell Responses

Analysis of *Foxp3*^{YFPcre}*Tgfb1*$^{Δ/Δ}$ mice revealed intense dysregulation of the Tfh cell response, characterized by increased frequencies of CD4$^+$CXCR5$^+$PD1$^+$ Tfh and B220$^+$GL-7$^+$ germinal center B cells as well as increased activation markers (CD80, CD86, and major histocompatibility complex [MHC] class II) on classic DCs in secondary lymphoid organs. T follicular Treg (Tfr) cell frequencies were similar to those of *Foxp3*^{YFPcre} mice, suggesting defective Tfh suppression by TGF-β1-deficient Tfr cells (Figures 7A–7D). In contrast, these abnormalities were largely absent in *Foxp3*^{YFPcre}*Tgfb1*$^{Δ/+}$ mice. The dysregulated Tfh response in *Foxp3*^{YFPcre}*Tgfb1*$^{Δ/Δ}$ mice was associated with increased autoantibody production involving all Ig isotypes, including IgE, whereas autoantibody production in *Foxp3*^{YFPcre}*Tgfb1*$^{Δ/+}$ and *Foxp3*^{YFPcre} mice was similar (Figure 7E; Figures S7A–S7C). Depletion of B cells by treatment with an anti-CD20 monoclonal antibody (mAb) prolonged the survival of *Foxp3*^{YFPcre}*Tgfb1*$^{Δ/Δ}$ mice (Figure 7F). These findings highlight the differential requirement for Treg cell-derived TGF-β1 in regulating allergic versus autoimmune antibody responses, with the latter being effectively controlled in mice with Treg cell-specific *Tgfb1* haploinsufficiency.

DISCUSSION

Our study demonstrates a pivotal role of Treg cell-derived TGF-β1 in regulating allergic and autoimmune responses, with a stepwise decrease in *Tgfb1* transcription in Treg cells precipitating contrasting immune-dysregulatory outcomes. Thus, an incremental decrease in *Tgfb1* transcription because of Th2 cell like-reprogramming of Treg cells, a pathologic process triggered by dysbiosis in FA subjects or enhanced IL-4R signaling in *Il4ra*^{F709} mice (Abdel-Gadir et al., 2019; Noval Rivas et al., 2015), promotes allergic dysregulation and susceptibility to FA. This outcome was phenocopied by Treg cell-specific *Tgfb1* haploinsufficiency or *Tgfb1* deletion by a partially penetrant, BAC-based, *Foxp3*-driven Cre recombinase and abrogated by *Tgfb1* overexpression in Treg cells of FA-prone *Il4ra*^{F709} mice. Importantly, the allergic dysregulation was linked to decreased expression of *Tgfb1* in gut Treg cells, whose upregulation by the commensal microbiota was essential for their differentiation into oral tolerance-promoting ROR-γt$^+$ Treg cells. In contrast, homozygous *Tgfb1* deficiency in Treg cells precipitated fatal autoimmunity related to Tfh cell and DC dysregulation, an outcome echoed in rare patients with biallelic loss-of-function mutations in *Tgfb1* (Kotlarz et al., 2018). Overall, these results establish that Treg cell-derived TGF-β1 differentially regulates allergic and autoimmune responses in a Treg cell *Tgfb1* gene dose- and microbiota-dependent manner.

A key aspect of our study was demonstration of a privileged role of Treg cell-derived TGF-β1 in maintenance of oral and peripheral tolerance. The original paradigm for differentiation of antigen-specific iTreg cells in the gut stipulated dependence of this process on TGF-β1 derived from specialized CD103$^+$ antigen-presenting DCs (Coombes et al., 2007; Sun et al., 2007). Our results indicate an additional non-redundant role of Treg cell-derived TGF-β1 in further differentiation of these cells into oral tolerance-promoting RORγt$^+$ Treg cells, whose deficiency results in profound allergic dysregulation (Abdel-Gadir et al., 2019; Ohnmacht et al., 2015). The action of Treg cell-derived TGF-β1 in promoting RORγt$^+$ Treg cell differentiation appeared to be cell intrinsic, as evidenced by failure of such differentiation upon Treg cell-specific deletion of *Tgfbr2*. The finding that commensals upregulated *Tgfb1* expression in gut Treg cells points to a commensal-regulated Treg cell TGF-β1-RORγt axis operative in mucosal tolerance and relevant to the weaning reaction, whose disruption by dysbiosis gives rise to allergic dysregulation and FA (Abdel-Gadir et al., 2019; Al Nabhani et al., 2019).

Treg cell *Tgfb1* haploinsufficiency gave rise to profound gut tissue mast cell expansion and a steep increase in serum IgE concentrations conducive to intense anaphylactic responses upon oral allergen challenge. *In vitro* assays revealed that TGF-β1 deficiency impaired the capacity of Treg cells to suppress mast cell activation. Of particular interest was the finding that

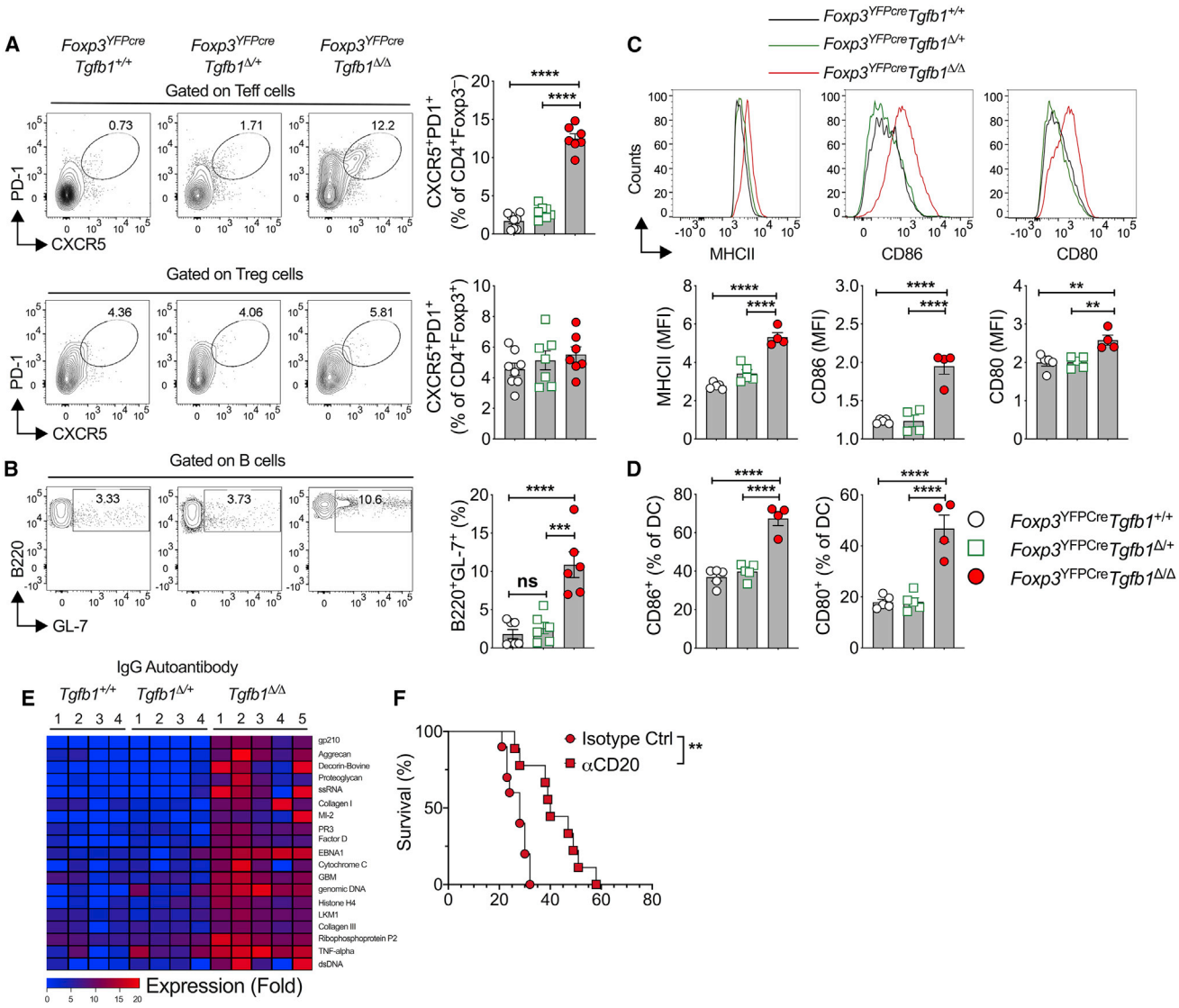

Figure 7. Treg Cell *Tgfb1* Gene Dose-Dependent Regulation of Autoimmune Humoral Responses

(A) Flow cytometry analysis and frequencies of CXCR5 and PD-1 expression in splenic Teff and Treg cells.

(B) Flow cytometry analysis and frequencies of germinal center B cells ($B220^+GL\text{-}7^+$) within the splenic B cell population.

(C) Frequencies of CD80- and CD86-expressing cells within $CD11c^+MHCII^+$ splenic DC population.

(D) Flow cytometry analysis and MFI of MHC class II, CD80, and CD86 expression within the $CD11c^+$MHC class II^+ splenic DC population.

(E) Heatmap representation of serum IgG autoantibodies in littermate mice of the respective genotypes.

(F) Survival curves of $Foxp3^{YFPcre}Tgfb1^{\Delta/\Delta}$ mice treated with the isotype control or anti-CD20 mAb.

The age of the mice was between 3 and 4 weeks of age. Each symbol or column number represents an independent sample. Numbers in flow plots indicate percentages. Error bars indicate SEM. Statistical tests: one-way ANOVA with Dunnett's post hoc analysis (A–D), R package "limma" and multiple comparisons corrections adjusted to $p < 0.05$ (E), and log rank test (F). *$p < 0.05$, **$p < 0.01$, ****$p < 0.0001$. Data are representative of 2–3 independent experiments with 4–8 mice per group. See also Figure S7.

deletion of *Tgfbr2* in mast cells precipitated susceptibility to FA, emphasizing the role of TGF-β1 signaling in restraining mast cell responses (Gomez et al., 2005). The essential role of $ROR\gamma t^+$ Treg cells in this process may relate to enrichment of LAP expression in this subpopulation pursuant to its induction by the microbiota and also to the biased response by this population to gut-derived microbial and food antigens (Abdel-Gadir et al., 2019; Ohnmacht et al., 2015).

Although Treg cell *Tgfb1* haploinsufficieny precipitated allergic dysregulation, biallelic *Tgfb1* deletion resulted in systemic lymphoproliferation and autoimmunity. Previous studies have identified a critical role of TGF-β1 in suppressing autoimmunity by employing mouse models of global and T cell-specific *Tgfb1* deletion and have also implicated TGF-β signaling in T cells and DCs in such regulation (Gorelik and Flavell, 2000; Gutcher et al., 2011; Li et al., 2007; Marie et al., 2005; Ramalingam

et al., 2012; Shull et al., 1992). Our study specifically identifies Treg cells as the critical source of TGF-β1 in enforcing peripheral tolerance and restraining autoimmunity. Biallelic *Tgfb1* deletion in Treg cells unleashed intense DC dysregulation, Teff cell activation, and autoantibody production. The latter phenotype was associated with heightened Tfh and germinal center B cell responses and dysregulated DC activation. These abnormalities were largely absent in $Foxp3^{YFPcre}Tgfb1^{\Delta/+}$ mice, consistent with the capacity of *Tgfb1* haploinsufficient Treg cells to restrain these pathogenic autoimmune responses. This dichotomy in the regulation of allergic versus autoimmune responses points to distinct checkpoints governing regulation by Treg cells of the respective immune responses in a *Tgfb1* gene dose-dependent manner. Previous studies have linked deletion of *Tgfbr2* in $CD4^+$ T cells with Tfh cell dysregulation by a mechanism involving loss of Treg cell TGF-β1-mediated suppression of Tfh cells (McCarron and Marie, 2014). Our results indicate that Treg cells are a critical source of TGF-β1 mediating regulation of Tfh cell responses whose loss engenders dysregulated autoantibody production.

Although the essential role of $CD4^+$ T cell-derived TGF-β1 in peripheral tolerance has been established previously, the contribution of Treg cell-derived TGF-β1 to peripheral tolerance remained unclear. A previous study employed a complex targeting approach to deplete TGF-β1 expression in Treg cells. This approach involved deletion of a different floxed *Tgfb1* allele with $Foxp3^{YFPcre}$ and inactivation of the other allele by insertion of in-frame EGFP cDNA into exon 1 of *Tgfb1* (Gutcher et al., 2011). The resulting mice were healthy, but their Treg cell frequency was increased, suggesting that Treg cell-derived TGF-β1 plays a role in controlling Treg cell homeostasis. These results echoed those we obtained with BAC-$Foxp3^{EGFPcre}Tgfb1^{\Delta/\Delta}$ mice, suggesting incomplete deletion of the floxed allele, hypomorphic function of the $Tgfb1^{EGFP}$ allele, and/or permissiveness of the exon 1 targeting strategy for expression of a TGF-β1 peptide from a downstream open reading frame. Overall, the fatal autoimmunity observed in $Foxp3^{YFPcre}Tgfb1^{\Delta/\Delta}$ mice, which, unlike the BAC-$Foxp3^{EGFPcre}Tgfb1^{\Delta/\Delta}$ mice, do not show evidence of Treg cell escape from *Tgfb1* deletion, argues for an essential, non-redundant role of Treg cell *Tgfb1* in peripheral tolerance. Notwithstanding the abundance of TGF-β production in different tissues and by different cell types, our results further emphasize the importance of the context of TGF-β action in orchestrating unique immune responses, as demonstrated recently for migratory DC-activated TGF-β in preconditioning naive CD8 T cells to become epithelial tissue-resident cells (Mani et al., 2019).

In conclusion, our study reveals the primacy of Treg cells as a source of TGF-β1 in immunoregulation and outlines genetic and environmental mechanisms by which Treg cell-derived TGF-β1 can separately exercise control over allergic and autoimmune responses.

STAR★METHODS

Detailed methods are provided in the online version of this paper and include the following:

- KEY RESOURCES TABLE
- RESOURCE AVAILABILITY
  - Lead Contact
  - Materials Availability
  - Data and Code Availability
- EXPERIMENTAL MODEL AND SUBJECT DETAILS
  - Mice
  - Human study population
- METHOD DETAILS
  - Sensitization and challenge protocol
  - ATAC-Seq
  - Chromatin Immunoprecipitation
  - Plasmids and reagents
  - Luciferase assay
  - Isolation of Spleen, MLN and LP lymphocytes
  - Flow cytometry
  - Quantitative real-time PCR for host immunological Targets
  - Bacterial consortia
  - ELISA
  - TGF-β1 ELISA assays
  - Histology
  - Autoantibody array analysis
  - B cell depletion
  - Mast cell suppression assay
  - Treg cells adoptive transfer
- QUANTIFICATION AND STATISTICAL ANALYSIS

SUPPLEMENTAL INFORMATION

Supplemental Information can be found online at https://doi.org/10.1016/j.immuni.2020.10.002.

ACKNOWLEDGMENTS

This work was supported by NIH NIAID grants 5R01AI1269151 and 5R01AI085090 (to T.A.C.) and 5R01AI119918 (to H.C.O), NIDDK grants P30DK056338 (to L.B.) and T32 AI007512 (O.T.B.), the Rao Chakravorti Family Fund (to H.C.O.), the Bunning Foundation (to H.C.O. and T.C.), and DBT/Wellcome Trust India Alliance Intermediate Fellowship IA/I/19/1/504276 (to K.B.).

AUTHOR CONTRIBUTIONS

J.A.T., E.S.-V., M.N.R., S.W., and T.C. designed experiments. J.A.T., M.N.R., S.W., J.J.H.F., M.B., A.A.-G., H.H., Y.C., O.T.B., L.-M.C., M.F., and R.L.C. performed experiments and developed experimental models. K.B. analyzed the ATAC-seq data, and C.Z. and Q.-Z.L. analyzed the autoantibody arrays. L.B. provided the Clostridiales consortium. H.C.O. and P.T.S. provided scientific input regarding mast cell and Tfh experiments, respectively. E.C. and R.R. recruited food-allergic and control subjects and provided patient histories and blood samples. E.S.-V., J.A.T., and T.C. wrote the manuscript.

DECLARATION OF INTERESTS

L.B., T.C., A.A.-G., and R.R. are inventors on published US patent no. US10391131B2, submitted by The Brigham and Women's Hospital, Inc. and Children's Medical Center Corporation, which covers methods and compositions for prevention and treatment of food allergy using microbial treatments. T.C, E.S.-V., A.A.-G. and R.R. have pending patent applications related to the use of probiotics in enforcing oral tolerance in food allergy (no. 62/798,224). L.B., T.C., and R.R. are co-founders of and/or have equity in Paretobio.

Received: January 29, 2020
Revised: June 29, 2020
Accepted: September 30, 2020
Published: October 20, 2020; corrected online: November 20, 2020

REFERENCES

Abdel-Gadir, A., Schneider, L., Casini, A., Charbonnier, L.M., Little, S.V., Harrington, T., Umetsu, D.T., Rachid, R., and Chatila, T.A. (2018). Oral immunotherapy with omalizumab reverses the Th2 cell-like programme of regulatory T cells and restores their function. Clin. Exp. Allergy *48*, 825–836.

Abdel-Gadir, A., Stephen-Victor, E., Gerber, G.K., Noval Rivas, M., Wang, S., Harb, H., Wang, L., Li, N., Crestani, E., Spielman, S., et al. (2019). Microbiota therapy acts via a regulatory T cell MyD88/RORγt pathway to suppress food allergy. Nat. Med. *25*, 1164–1174.

Al Nabhani, Z., Dulauroy, S., Marques, R., Cousu, C., Al Bounny, S., Dejardin, F., Sparwasser, T., Berard, M., Cerf-Bensussan, N., and Eberl, G. (2019). A Weaning Reaction to Microbiota Is Required for Resistance to Immunopathologies in the Adult. Immunity *50*, 1276–1288.e5.

Apostolou, I., and von Boehmer, H. (2004). In vivo instruction of suppressor commitment in naive T cells. J. Exp. Med. *199*, 1401–1408.

Azhar, M., Yin, M., Bommireddy, R., Duffy, J.J., Yang, J., Pawlowski, S.A., Boivin, G.P., Engle, S.J., Sanford, L.P., Grisham, C., et al. (2009). Generation of mice with a conditional allele for transforming growth factor beta 1 gene. Genesis *47*, 423–431.

Bach, J.F. (2002). The effect of infections on susceptibility to autoimmune and allergic diseases. N. Engl. J. Med. *347*, 911–920.

Bach, J.F. (2018). The hygiene hypothesis in autoimmunity: the role of pathogens and commensals. Nat. Rev. Immunol. *18*, 105–120.

Buenrostro, J.D., Wu, B., Chang, H.Y., and Greenleaf, W.J. (2015). ATAC-seq: A Method for Assaying Chromatin Accessibility Genome-Wide. Curr. Protoc. Mol. Biol. *109*, 21.29.1–21.29.9.

Burton, O.T., Darling, A.R., Zhou, J.S., Noval-Rivas, M., Jones, T.G., Gurish, M.F., Chatila, T.A., and Oettgen, H.C. (2013). Direct effects of IL-4 on mast cells drive their intestinal expansion and increase susceptibility to anaphylaxis in a murine model of food allergy. Mucosal Immunol. *6*, 740–750.

Burton, O.T., Noval Rivas, M., Zhou, J.S., Logsdon, S.L., Darling, A.R., Koleoglou, K.J., Roers, A., Houshyar, H., Crackower, M.A., Chatila, T.A., and Oettgen, H.C. (2014). Immunoglobulin E signal inhibition during allergen ingestion leads to reversal of established food allergy and induction of regulatory T cells. Immunity *41*, 141–151.

Charbonnier, L.M., Cui, Y., Stephen-Victor, E., Harb, H., Lopez, D., Bleesing, J.J., Garcia-Lloret, M.I., Chen, K., Ozen, A., Carmeliet, P., et al. (2019). Functional reprogramming of regulatory T cells in the absence of Foxp3. Nat. Immunol. *20*, 1208–1219.

Coombes, J.L., Siddiqui, K.R., Arancibia-Cárcamo, C.V., Hall, J., Sun, C.M., Belkaid, Y., and Powrie, F. (2007). A functionally specialized population of mucosal CD103+ DCs induces Foxp3+ regulatory T cells via a TGF-beta and retinoic acid-dependent mechanism. J. Exp. Med. *204*, 1757–1764.

Cuende, J., Liénart, S., Dedobbeleer, O., van der Woning, B., De Boeck, G., Stockis, J., Huygens, C., Colau, D., Somja, J., Delvenne, P., et al. (2015). Monoclonal antibodies against GARP/TGF-β1 complexes inhibit the immunosuppressive activity of human regulatory T cells in vivo. Sci. Transl. Med. *7*, 284ra56.

Edwards, J.P., Hand, T.W., Morais da Fonseca, D., Glass, D.D., Belkaid, Y., and Shevach, E.M. (2016). The GARP/Latent TGF-β1 complex on Treg cells modulates the induction of peripherally derived Treg cells during oral tolerance. Eur. J. Immunol. *46*, 1480–1489.

Esterházy, D., Loschko, J., London, M., Jove, V., Oliveira, T.Y., and Mucida, D. (2016). Classical dendritic cells are required for dietary antigen-mediated induction of peripheral T(reg) cells and tolerance. Nat. Immunol. *17*, 545–555.

Gomez, G., Ramirez, C.D., Rivera, J., Patel, M., Norozian, F., Wright, H.V., Kashyap, M.V., Barnstein, B.O., Fischer-Stenger, K., Schwartz, L.B., et al. (2005). TGF-beta 1 inhibits mast cell Fc epsilon RI expression. J. Immunol. *174*, 5987–5993.

Gorelik, L., and Flavell, R.A. (2000). Abrogation of TGFbeta signaling in T cells leads to spontaneous T cell differentiation and autoimmune disease. Immunity *12*, 171–181.

Grant, C.R., Liberal, R., Mieli-Vergani, G., Vergani, D., and Longhi, M.S. (2015). Regulatory T-cells in autoimmune diseases: challenges, controversies and–yet–unanswered questions. Autoimmun. Rev. *14*, 105–116.

Grützkau, A., Smorodchenko, A., Lippert, U., Kirchhof, L., Artuc, M., and Henz, B.M. (2004). LAMP-1 and LAMP-2, but not LAMP-3, are reliable markers for activation-induced secretion of human mast cells. Cytometry A *61*, 62–68.

Gutcher, I., Donkor, M.K., Ma, Q., Rudensky, A.Y., Flavell, R.A., and Li, M.O. (2011). Autocrine transforming growth factor-β1 promotes in vivo Th17 cell differentiation. Immunity *34*, 396–408.

Hall, B.E., Zheng, C., Swaim, W.D., Cho, A., Nagineni, C.N., Eckhaus, M.A., Flanders, K.C., Ambudkar, I.S., Baum, B.J., and Kulkarni, A.B. (2010). Conditional overexpression of TGF-beta1 disrupts mouse salivary gland development and function. Lab. Invest. *90*, 543–555.

Harb, H., Amarasekera, M., Ashley, S., Tulic, M.K., Pfefferle, P.I., Potaczek, D.P., Martino, D., Kesper, D.A., Prescott, S.L., and Renz, H. (2015). Epigenetic Regulation in Early Childhood: A Miniaturized and Validated Method to Assess Histone Acetylation. Int. Arch. Allergy Immunol. *168*, 173–181.

Haribhai, D., Lin, W., Edwards, B., Ziegelbauer, J., Salzman, N.H., Carlson, M.R., Li, S.H., Simpson, P.M., Chatila, T.A., and Williams, C.B. (2009). A central role for induced regulatory T cells in tolerance induction in experimental colitis. J. Immunol. *182*, 3461–3468.

Heintzman, N.D., Stuart, R.K., Hon, G., Fu, Y., Ching, C.W., Hawkins, R.D., Barrera, L.O., Van Calcar, S., Qu, C., Ching, K.A., et al. (2007). Distinct and predictive chromatin signatures of transcriptional promoters and enhancers in the human genome. Nat. Genet. *39*, 311–318.

Heinz, S., Benner, C., Spann, N., Bertolino, E., Lin, Y.C., Laslo, P., Cheng, J.X., Murre, C., Singh, H., and Glass, C.K. (2010). Simple combinations of lineage-determining transcription factors prime cis-regulatory elements required for macrophage and B cell identities. Mol. Cell *38*, 576–589.

Kaplan, M.H., Schindler, U., Smiley, S.T., and Grusby, M.J. (1996). Stat6 is required for mediating responses to IL-4 and for development of Th2 cells. Immunity *4*, 313–319.

Konkel, J.E., Zhang, D., Zanvit, P., Chia, C., Zangarle-Murray, T., Jin, W., Wang, S., and Chen, W. (2017). Transforming Growth Factor-β Signaling in Regulatory T Cells Controls T Helper-17 Cells and Tissue-Specific Immune Responses. Immunity *46*, 660–674.

Kotlarz, D., Marquardt, B., Barøy, T., Lee, W.S., Konnikova, L., Hollizeck, S., Magg, T., Lehle, A.S., Walz, C., Borggraefe, I., et al. (2018). Human TGF-β1 deficiency causes severe inflammatory bowel disease and encephalopathy. Nat. Genet. *50*, 344–348.

Langmead, B., and Salzberg, S.L. (2012). Fast gapped-read alignment with Bowtie 2. Nat. Methods *9*, 357–359.

Li, M.O., Wan, Y.Y., and Flavell, R.A. (2007). T cell-produced transforming growth factor-beta1 controls T cell tolerance and regulates Th1- and Th17-cell differentiation. Immunity *26*, 579–591.

Liénart, S., Merceron, R., Vanderaa, C., Lambert, F., Colau, D., Stockis, J., van der Woning, B., De Haard, H., Saunders, M., Coulie, P.G., et al. (2018). Structural basis of latent TGF-β1 presentation and activation by GARP on human regulatory T cells. Science *362*, 952–956.

Lin, W., Truong, N., Grossman, W.J., Haribhai, D., Williams, C.B., Wang, J., Martín, M.G., and Chatila, T.A. (2005). Allergic dysregulation and hyperimmunoglobulinemia E in Foxp3 mutant mice. J. Allergy Clin. Immunol. *116*, 1106–1115.

Mani, V., Bromley, S.K., Äijö, T., Mora-Buch, R., Carrizosa, E., Warner, R.D., Hamze, M., Sen, D.R., Chasse, A.Y., Lorant, A., et al. (2019). Migratory DCs activate TGF-β to precondition naïve $CD8^+$ T cells for tissue-resident memory fate. Science *366*, eaav5728.

Marie, J.C., Letterio, J.J., Gavin, M., and Rudensky, A.Y. (2005). TGF-beta1 maintains suppressor function and Foxp3 expression in CD4+CD25+ regulatory T cells. J. Exp. Med. *201*, 1061–1067.

McCarron, M.J., and Marie, J.C. (2014). TGF-β prevents T follicular helper cell accumulation and B cell autoreactivity. J. Clin. Invest. *124*, 4375–4386.

Mucida, D., Kutchukhidze, N., Erazo, A., Russo, M., Lafaille, J.J., and Curotto de Lafaille, M.A. (2005). Oral tolerance in the absence of naturally occurring Tregs. J. Clin. Invest. *115*, 1923–1933.

Murphy, K.M., Heimberger, A.B., and Loh, D.Y. (1990). Induction by antigen of intrathymic apoptosis of CD4+CD8+TCRlo thymocytes in vivo. Science *250*, 1720–1723.

Nasrallah, R., Imianowski, C.J., Bossini-Castillo, L., Grant, F.M., Dogan, M., Placek, L., Kozhaya, L., Kuo, P., Sadiyah, F., Whiteside, S.K., et al. (2020). A distal enhancer at risk locus 11q13.5 promotes suppression of colitis by T_{reg} cells. Nature *583*, 447–452.

Noval Rivas, M., Burton, O.T., Wise, P., Charbonnier, L.M., Georgiev, P., Oettgen, H.C., Rachid, R., and Chatila, T.A. (2015). Regulatory T cell reprogramming toward a Th2-cell-like lineage impairs oral tolerance and promotes food allergy. Immunity *42*, 512–523.

Noval Rivas, M., Burton, O.T., Wise, P., Zhang, Y.Q., Hobson, S.A., Garcia Lloret, M., Chehoud, C., Kuczynski, J., DeSantis, T., Warrington, J., et al. (2013). A microbiota signature associated with experimental food allergy promotes allergic sensitization and anaphylaxis. J. Allergy Clin. Immunol. *131*, 201–212.

Noval Rivas, M., and Chatila, T.A. (2016). Regulatory T cells in allergic diseases. J. Allergy Clin. Immunol. *138*, 639–652.

Ohnmacht, C., Park, J.H., Cording, S., Wing, J.B., Atarashi, K., Obata, Y., Gaboriau-Routhiau, V., Marques, R., Dulauroy, S., Fedoseeva, M., et al. (2015). MUCOSAL IMMUNOLOGY. The microbiota regulates type 2 immunity through $ROR\gamma t^+$ T cells. Science *349*, 989–993.

Platts-Mills, T.A. (2015). The allergy epidemics: 1870-2010. J. Allergy Clin. Immunol. *136*, 3–13.

Ramalingam, R., Larmonier, C.B., Thurston, R.D., Midura-Kiela, M.T., Zheng, S.G., Ghishan, F.K., and Kiela, P.R. (2012). Dendritic cell-specific disruption of TGF-β receptor II leads to altered regulatory T cell phenotype and spontaneous multiorgan autoimmunity. J. Immunol. *189*, 3878–3893.

Ramírez, F., Dündar, F., Diehl, S., Grüning, B.A., and Manke, T. (2014). deepTools: a flexible platform for exploring deep-sequencing data. Nucleic Acids Res. *42*, W187-91.

Ritchie, M.E., Phipson, B., Wu, D., Hu, Y., Law, C.W., Shi, W., and Smyth, G.K. (2015). limma powers differential expression analyses for RNA-sequencing and microarray studies. Nucleic Acids Res. *43*, e47.

Robinson, J.T., Thorvaldsdóttir, H., Winckler, W., Guttman, M., Lander, E.S., Getz, G., and Mesirov, J.P. (2011). Integrative genomics viewer. Nat. Biotechnol. *29*, 24–26.

Rubtsov, Y.P., Rasmussen, J.P., Chi, E.Y., Fontenot, J., Castelli, L., Ye, X., Treuting, P., Siewe, L., Roers, A., Henderson, W.R., Jr., et al. (2008). Regulatory T cell-derived interleukin-10 limits inflammation at environmental interfaces. Immunity *28*, 546–558.

Scholten, J., Hartmann, K., Gerbaulet, A., Krieg, T., Müller, W., Testa, G., and Roers, A. (2008). Mast cell-specific Cre/loxP-mediated recombination in vivo. Transgenic Res. *17*, 307–315.

Sefik, E., Geva-Zatorsky, N., Oh, S., Konnikova, L., Zemmour, D., McGuire, A.M., Burzyn, D., Ortiz-Lopez, A., Lobera, M., Yang, J., et al. (2015). MUCOSAL IMMUNOLOGY. Individual intestinal symbionts induce a distinct population of $ROR\gamma^+$ regulatory T cells. Science *349*, 993–997.

Shull, M.M., Ormsby, I., Kier, A.B., Pawlowski, S., Diebold, R.J., Yin, M., Allen, R., Sidman, C., Proetzel, G., Calvin, D., et al. (1992). Targeted disruption of the mouse transforming growth factor-beta 1 gene results in multifocal inflammatory disease. Nature *359*, 693–699.

Srinivas, S., Watanabe, T., Lin, C.S., William, C.M., Tanabe, Y., Jessell, T.M., and Costantini, F. (2001). Cre reporter strains produced by targeted insertion of EYFP and ECFP into the ROSA26 locus. BMC Dev. Biol. *1*, 4.

Stephen-Victor, E., Crestani, E., and Chatila, T.A. (2020). Dietary and Microbial Determinants in Food Allergy. Immunity *53*, 277–289.

Sun, C.M., Hall, J.A., Blank, R.B., Bouladoux, N., Oukka, M., Mora, J.R., and Belkaid, Y. (2007). Small intestine lamina propria dendritic cells promote de novo generation of Foxp3 T reg cells via retinoic acid. J. Exp. Med. *204*, 1775–1785.

Tachdjian, R., Al Khatib, S., Schwinglshackl, A., Kim, H.S., Chen, A., Blasioli, J., Mathias, C., Kim, H.Y., Umetsu, D.T., Oettgen, H.C., and Chatila, T.A. (2010). In vivo regulation of the allergic response by the IL-4 receptor alpha chain immunoreceptor tyrosine-based inhibitory motif. J. Allergy Clin. Immunol. *125*, 1128–1136.e8.

Tran, D.Q., Andersson, J., Wang, R., Ramsey, H., Unutmaz, D., and Shevach, E.M. (2009). GARP (LRRC32) is essential for the surface expression of latent TGF-beta on platelets and activated FOXP3+ regulatory T cells. Proc. Natl. Acad. Sci. USA *106*, 13445–13450.

Travis, M.A., and Sheppard, D. (2014). TGF-β activation and function in immunity. Annu. Rev. Immunol. *32*, 51–82.

Voehringer, D., Wu, D., Liang, H.E., and Locksley, R.M. (2009). Efficient generation of long-distance conditional alleles using recombineering and a dual selection strategy in replicate plates. BMC Biotechnol. *9*, 69.

Wu, D., Luo, Y., Guo, W., Niu, Q., Xue, T., Yang, F., Sun, X., Chen, S., Liu, Y., Liu, J., et al. (2017). Lkb1 maintains T_{reg} cell lineage identity. Nat. Commun. *8*, 15876.

Yeh, H.W., Hsu, E.C., Lee, S.S., Lang, Y.D., Lin, Y.C., Chang, C.Y., Lee, S.Y., Gu, D.L., Shih, J.H., Ho, C.M., et al. (2018). PSPC1 mediates TGF-β1 autocrine signalling and Smad2/3 target switching to promote EMT, stemness and metastasis. Nat. Cell Biol. *20*, 479–491.

Zhou, X., Jeker, L.T., Fife, B.T., Zhu, S., Anderson, M.S., McManus, M.T., and Bluestone, J.A. (2008). Selective miRNA disruption in T reg cells leads to uncontrolled autoimmunity. J. Exp. Med. *205*, 1983–1991.

STAR★METHODS

KEY RESOURCES TABLE

REAGENT or RESOURCE	SOURCE	IDENTIFIER
Antibodies		
eBioscience Fixable Viability Dye eFluor 506 and eFluor 780	Thermo Fischer	Cat# 65-0866-18
APC-Cy7 and FITC anti-mouse CD3 Antibody	Biolegend	Cat# 100222
		Cat# 100204
Brilliant Violet 605 anti-mouse CD4 Antibody	Biolegend	Cat# 100451
PE anti-mouse IgE Antibody	Biolegend	Cat# 406908
Brilliant Violet 605 anti-mouse CD86 Antibody	Biolegend	Cat# 105036
Brilliant Violet 421 anti-human/mouse/rat CD278 (ICOS) Antibody	Biolegend	Cat# 313524
PE and APC anti-mouse LAP (TGF-β1) Antibody	Biolegend	Cat# 141404
		Cat# 141406
Alexa Fluor® 488 and APC anti-mouse/human CD45R/ B220 Antibody	Biolegend	Cat# 103225
		Cat# 103212
PE/Cyanine7 anti-mouse CD117 (c-Kit) Antibody	Biolegend	Cat# 105814
PE and PE/Dazzle 594 anti-mouse IL-4 Antibody	Biolegend	Cat# 504104
		Cat# 504132
PE/Cyanine7 anti-mouse IL-17A Antibody	Biolegend	Cat# 506922
APC anti-mouse IFN-γ Antibody	Biolegend	Cat# 505810
FITC anti-mouse Ly-6G/Ly-6C (Gr-1) Antibody	Biolegend	Cat# 108406
Alexa Fluor® 647 anti-mouse Ly-6C Antibody	Biolegend	Cat# 128010
FITC anti-mouse CD19 Antibody	Biolegend	Cat# 115506
FITC anti-mouse I-Ad Antibody	Biolegend	Cat# 115006
Brilliant Violet 605 anti-mouse CD45 Antibody	Biolegend	Cat# 103140
PE anti-mouse CD152 (CTLA-4) Antibody	Biolegend	Cat# 106306
Alexa Fluor® 647 anti-mouse CD279 (PD-1) Antibody	Biolegend	Cat# 109118
APC anti-mouse CD107a (LAMP-1) Antibody	Biolegend	Cat# MA5-28671
FITC and PE anti mouse CD11b Antibody	Thermo Fischer	Cat# 11-0112-82
		Cat# 12-0112-82
APC anti-mouse FceR1 alpha Antibody	Thermo Fischer	Cat# 121614
FITC and PE anti mouse CD11c Antibody	Thermo Fischer	Cat# 11-0114-82
		Cat# 25-0114-82
eFluor 610 anti-mouse CD185 (CXCR5) Antibody	Thermo Fischer	Cat# 61-7185-82
eFluor 450 anti-mouse CD44 Antibody	Thermo Fischer	Cat# 48-0441-82
APC anti-mouse CD62L Antibody	Thermo Fischer	Cat# 17-0621-82
APC anti-mouse CD134 (OX40) Antibody	Thermo Fischer	Cat# 17-5905-82
PE anti-mouse GL7 Antibody	Thermo Fischer	Cat# 12-5902-82
PE/Cyanine7 anti-mouse GARP Antibody	Thermo Fischer	Cat# 25-9891-82
PE anti-mouse CD80 Antibody	Thermo Fischer	Cat# 12-0801-82
PE/Cyanine7 anti-mouse CD25 Antibody	Thermo Fischer	Cat# 25-0251-82
APC-eFluor 780 anti-mouse HELIOS Antibody	Thermo Fischer	Cat# 47-9883-42
eFluor 660 and PerCP-eFluor 710 anti-mouse GATA3 Antibody	Thermo Fischer	Cat# 50-9966-42
		Cat# 46-9966-42
PE anti-mouse Ki-67 Antibody	Thermo Fischer	Cat# 12-5698-82
PE anti-mouse Neuropilin-1 (CD304) Antibody	Thermo Fischer	Cat# 12-3041-82

(*Continued on next page*)

Continued

REAGENT or RESOURCE	SOURCE	IDENTIFIER
PE anti-mouse RORγt Antibody	Thermo Fischer	Cat# 12-6981-82
BV421 Anti-Mouse RORγt Antibody	BD Biosciences	Cat# 562894
PE/Cyanine7 anti-human CD127 (IL-7Rα) Antibody	Biolegend	Cat# 351320
APC/Cyanine7 anti-human CD3 Antibody	Biolegend	Cat# 344818
PE anti-human LAP (TGF-β1) Antibody	Biolegend	Cat# 349704
PerCP-Cyanine5.5 anti-human CD4 Antibody	Thermo Fischer	Cat# 45-0049-42
APC anti-human FOXP3 Antibody	Thermo Fischer	Cat# 17-4776-42
FITC anti-human CD25 Antibody	BD Biosciences	Cat# 347643
Critical Commercial Assays		
MCPT-1 (mMCP-1) Mouse Uncoated ELISA Kit	Thermo fisher	Cat# 7400488-7503-86
Mouse TGF-beta 1 DuoSet ELISA	R&D Systems	Cat# DY1679-05
RNeasy Mini Kit	QIAGEN	Cat# 74106
Q5® Site-Directed Mutagenesis Kit	NEB	Cat# E0554S
Plasmid	Addgene	Cat# 101762
Experimental Models: Organisms/Strains		
BALB/cByJ	Jax	Stock No: 000651
Il4ra^{F709}*Foxp3*^{YFPcre}	Talal Chatila, Boston Children's Hospital	N/A
Foxp3^{EGFPcre}*R26*$^{YFP/YFP}$	In this paper	N/A
Foxp3^{EGFPcre}*Tgfb1*$^{fl/fl}$*R26*$^{YFP/YFP}$	In this paper	N/A
Foxp3^{YFPcre}	Jax	Stock No: 016959
Il4ra^{F709}*Foxp3*^{YFPcre}*Il4-Il13*$^{fl/fl}$	PMID: 25769611	N/A
Il4ra^{F709}*Foxp3*^{YFPcre}*Tgfb1*^{Tg}	In this paper	N/A
Il4ra^{F709}*Foxp3*^{YFPcre} *Stat6*$^{-/-}$	PMID: 25769611	N/A
Foxp3^{YFPcre}*Tgfb1*$^{fl/fl}$	In this paper	N/A
DO11.10	Jax	N/A
DO11.10Foxp3^{EGFPcre}*Tgfb1*$^{fl/fl}$	In this paper	N/A
Mcpt5^{cre}*Tgfbr2*$^{\Delta/\Delta}$	In this paper	N/A
Foxp3^{YFPcre}*Tgfbr2*$^{\Delta/\Delta}$	PMID: 28423340	N/A
Foxp3^{EGFPcre}	Jax	Stock No: 023161
Tgfb1$^{fl/fl}$	Jax	Stock No: 010721
Oligonucleotides		
Tgfb1 TaqMan Assays	Thermo Fisher	Mm00441729_g1
Tgfb2 TaqMan Assays	Thermo Fisher	Mm00436955_m1
Tgfb3 TaqMan Assays	Thermo Fisher	Mm00436960_m1
Software and Algorithms		
GraphPad Prism 7	GraphPad Software	N/A
FlowJo 10.4.2	Tree Star	https://www.flowjo.com/solutions/flowjo/downloads

RESOURCE AVAILABILITY

Lead Contact

Further information and requests for resources and reagents should be directed to and will be fulfilled by the Lead Contact, Talal A. Chatila (talal.chatila@childrens.harvard.edu).

Materials Availability

All unique/stable reagents generated in this study are available from the Lead Contact with a completed Materials Transfer Agreement.

Data and Code Availability

The ATAC-Seq data reported in Figure 1A of this article has been deposited in the GEO repository (accession number GSE158804) and will be available on January 1, 2021.

EXPERIMENTAL MODEL AND SUBJECT DETAILS

Mice

BALB/cByJ (WT) and all the following strains, except where indicated, were obtained from or rederived at the JAX lab. *C.129X1-Il4-ra*$^{tm3.1Tch}$ (*Il4ra*^{F709}) have been previously described (Noval Rivas et al., 2013; Tachdjian et al., 2010). *Tgfb1*$^{tm2.1Doe}$/J, NOD/ShiLt-Tg(*Foxp3-*^{EGFPcre})1cJbs/J (*Foxp3*^{EGFPcre}), B6.129X1-*Gt(ROSA)26Sor*$^{tm1(EYFP)Cos}$/J (*R26*$^{YFP/YFP}$) and B6.129(Cg)-*Foxp3*$^{tm4(YFP/icre)Ayr}$/J (*Foxp3*^{YFPcre}) were backcrossed 12 generations on BALB/cBYJ (Azhar et al., 2009; Rubtsov et al., 2008; Srinivas et al., 2001; Zhou et al., 2008). *C.129P2(Cg)-Il4-Il13*$^{tm1.1Lky}$ (*Il4-Il13*$^{fl/fl}$) mice were crossed with *Il4ra*^{F709}*Foxp3*^{YFPcre} mice as indicated (Noval Rivas et al., 2015; Voehringer et al., 2009). *C.129S2-Stat6*^{tm1Gru} (*Stat6*$^{-/-}$) mice were crossed with *Il4ra*^{F709}*Foxp3*^{YFPcre} mice (Kaplan et al., 1996). FVB/N-Tg(CAG-EGFP,TGFB1*)C8Kul/J (*Tgfb1*^{Tg}) mice were backcrossed on C57BL/6 for 6 generations (Hall et al., 2010). *DO11.10Foxp3*^{EGFPcre} were generated from the respective transgenic mice (Murphy et al., 1990). B6.Tg(*Mcpt5*^{cre}) and B6.*Foxp3*^{YFPcre} mice were interbred with B6;129-*Tgfbr2*^{tm1Karl}/J mice to create *Mcpt5*^{cre}*Tgfbr2*$^{\Delta/\Delta}$ and *Foxp3*^{YFPcre}*Tgfbr2*$^{\Delta/\Delta}$ mice, respectively (Burton et al., 2014; Scholten et al., 2008). Mice were maintained under specific pathogen-free conditions and used according to the guidelines of the institutional Animal Research Committee at the Boston Children's Hospital.

Human study population

Three groups of subjects, aged from 6 months to 20 years were recruited under a protocol approved by the Institutional Review Board at the Boston Children's Hospital: 1) healthy subjects without a history of FA or atopy (n = 6), 2) non-food allergic subjects with other atopic diseases (including asthma, atopic dermatitis and allergic rhinitis) (n = 27) and 3) subjects who have FA (n = 22), as determined by the World Allergy Organization diagnostic criteria (2010). Subject demographics and allergen reactivity are detailed in Table S1, and inclusion and exclusion criteria are detailed as previously described (Abdel-Gadir et al., 2019).

METHOD DETAILS

Sensitization and challenge protocol

Mice were treated intragastrically with either sterile PBS or OVA (Sigma-Aldrich) (250μg) together with 10μg SEB (Toxin Technology) in PBS (Treg) once weekly for 8 weeks (Abdel-Gadir et al., 2019). On week 9, mice were challenged intragastrically with 150 mg of OVA. Anaphylaxis was assessed by measuring changes in total body core temperature with transponders placed subcutaneously 2 days before challenge (IPTT-300; Bio Medic Data Systems) and a DAS-6001 console (Bio Medic Data Systems).

ATAC-Seq

20,000 Treg cells/sample were used for preparation of ATAC-seq libraries according to the protocol described previously; however, with few modifications (Buenrostro et al., 2015). Briefly, cells were suspended in 100 μL of cold hypotonic lysis buffer [10mM Tris-HCl (pH 7.5), 10mM NaCl, 3mM MgCl2 and 0.5% NP40], followed by immediate centrifugation at 550 g for 30 min and re-suspension of the pellet in 5 μL of transposition reaction mix [1 μL of Tagment DNA Enzyme and 2.5 μL of Tagment DNA Buffer from Nextera DNA Sample Prep Kit (Illumina), 1.5 μL H_2O]. The transposition reaction was incubated for 60 min at 37°C which led to fragmentation and tagging of DNA. For library preparation, 7-cycles of PCR were performed followed by selection of small fragments (less than 600bp) using SPRI beads. A second round of PCR (7-cycles) with similar conditions was performed in order to obtain the final library. Libraries were sequenced on the NextSeq 500 instrument to generate paired-end short reads (50bp, forward; 33bp, reverse). Paired-end sequencing reads were aligned to the mouse reference genome (mm10) using bowtie aligner version 2.2.9 (Langmead and Salzberg, 2012), followed by removal of reads with multiple alignments as well as reads mapping to mitochondrial DNA. De-duplication of reads was performed with picard (v2.8.0). makeTagDirectory command of Homer package (v4.9) was used to create the tag directory followed by identification of peaks using the 'factor' parameter in the find Peaks command (Heinz et al., 2010). For visualization of ATAC-seq data, replicate specific bam output files from picard were merged and converted into normalized bigwig format using the bamCoverage function in deepTools with options – fragmentLength 200 –normalizeUsingRPKM (Ramírez et al., 2014), and bigwig file was visualized on Integrative Genomics Viewer (IGV) (Robinson et al., 2011).

Chromatin Immunoprecipitation

Treg cells were sorted from either *Foxp3*^{YFPcre} or *Foxp3*^{YFPcre}*Il4ra*^{F709} mice. The cells were then kept for 8 min in 1 mL of 1% paraformaldehyde (PFA; Sigma-Aldrich) at room temperature (RT). Next, the sample incubated with lysis buffer I (5mM PIPES pH 8, 85mM KCl, 0,5% NP40 (Igepal-CA630), Protease Inhibitor) for 20 min at RT, and then centrifuged for 5 min at 7,870 g at RT. The pellet was lysed with lysis buffer II (10mM Tris-HCl pH 7,5, 150mM NaCl, 1% NP40 (Igepal-CA630), 1% DOC (Natrium Deoxycholate), 0,1% SDS, 1mM EDTA, Protease Inhibitor). The chromatin was further sonicated to a length of 25-500 bp using bioruptor (Diagenode, USA) for 35 cycles (30 s on, 30 s off). The chromatin was then precipitated using either IgG mock control, STAT6 (Cell Signaling Technology), H3K4me3 (Active Motif, USA) or H3k27me3 (Active Motif USA) histone methylation overnight. The chromatin was washed

twice with each of the different washing buffers [wash buffer I (20mM Tris-HCl pH 8, 150mM NaCl, 2mM EDTA, 0,1% SDS, 1% Triton X-100), wash buffer II (20mM Tris-HCl pH 8, 500mM NaCl, 2mM EDTA, 0,1% SDS, 1% Triton X-100) and wash buffer III (10mM Tris-HCl pH 8, 1% NP40 (Igepal-CA630) 1% DOC, 1mM EDTA, 0,25M LiCl)]. The chromatin was then cleaned using 1X TE buffer (10mM Tris-HCl pH 8, 1mM EDTA) and eluted using an elution buffer (1% SDS, 0,1M NaHCO3). The DNA was then cleaned using QIAquick PCR purification kit (QIAGEN, USA). The DNA was then used in polymerase chain reaction (PCR) were conducted with the relevant primers (Harb et al., 2015). PCR primers for putative STAT6 binding in the Tgfb1 promoter are: Forward – TCCTTGACACTCT CATCCGC and Reverse - GGCACTGTCTTCATCTTAGCG. Percent enrichment to the input control was calculated for each target locus and separately for mock (IgG), STAT6, H3K4me1 or H3k27me3 antibodies. Intra- and inter-assay coefficients of variation calculated for percent enrichment did not exceed 10%. All samples were processed according to the same standardized protocol and analyzed blinded and in a randomized order.

Plasmids and reagents

pGL3-*Tgfb1* was obtained from Addgene (Yeh et al., 2018). The mouse *Tgfb1* promoter plasmid was generated using C57BL/6 cDNA using the following primers: mWT*Tgfb1*-F: attaggtaccacatgagcagggcccactgt, mWT*Tgfb1*-R: taataagcttgcgaagggcggcggcggcgg. The *Tgfb1* promoter harboring a deletion of the STAT6 binding site was generated using the Q5 Site-Directed Mutagenesis Kit (NEB) and the following primer set: mMUT*Tgfb1*-f: ACATGAGCAGGGCCCACTGTTAAAGCGTGT, and mMUT*Tgfb1*-r: ACCCATGA GAAATACACGCTTTAACAGTGG. The sequences of both the native (*Tgfb1*^{STAT6}) and mutant (*Tgfb1*$^{\Delta STAT6}$) *Tgfb1* promoter plasmids were confirmed by Sanger sequencing.

Luciferase assay

EL4 cells were seeded in 6-well plates with non-antibiotic X-VIVO 15 medium and transfected with reporter gene plasmids as indicated. The total amount of DNA was kept constant. pTK-Renilla was co-transfected to normalize transfection efficiency. 24 hours (hr) post transfection, EL4 cells bearing the *Tgfb1*^{STAT6} or *Tgfb1*$^{\Delta STAT6}$ plasmid constructs were stimulated with 20ng/ml of mouse IL-4 for 24 hr before luciferase reporter assays were performed. Luciferase activity was analyzed with the Dual Luciferase Reporter Assay System (Promega).

Isolation of Spleen, MLN and LP lymphocytes

Spleen and MLNs were isolated and homogenized in PBS containing 2% FCS buffer. Red blood cells from splenic suspensions were lysed with ACK buffer. Cells were washed once with PBS containing 2% FCS and used for experiments. Small intestines were dissected from mice and the fecal contents were flushed out using PBS containing 2% FCS. Peyer's patch was excised and the intestines were cut into 1cm pieces and treated with PBS containing 2% FCS, 1.5 mM DTT, and 10mM EDTA at 37 °C for 30 min with constant stirring to remove mucous and epithelial cells. The tissues were then minced and the cells were dissociated in RPMI containing collagenase (2 mg/ml collagenase II; Worthington), DNase I (100 μg/ml; Sigma-Aldrich), 5mM $MgCl_2$, 5mM $CaCl_2$, 5mM HEPES, and 10% FBS with constant stirring at 37 °C for 45 min. Leukocytes were collected at the interface of a 40%/70% Percoll gradient (GE Healthcare). The cells were washed with PBS containing 2% FCS and used for experiments.

Flow cytometry

The following anti-mouse monoclonal antibodies (mAb) were used: CD3 (17A2), CD4 (RM4-5), IgE (RME-1), LAMP-1 (1D4B), CD86 (GL-1), CTLA-4 (UC10-4B9), ICOS (C398.4A), LAP (TW7-16B4), B220 (A3-6B2), cKit (2B8), IL-4 (11B11), IL-17a (TC11-18H10.1), IFN-γ (XMG1.2), Gr-1 (RB6-8C5), CD11b (M1/70), CD19 (6D5), I-Ad (39-10-8), CD45 (30-F11), and Ly-6C (HK1.4) were from Biolegend. Foxp3 (FJK-16S), GATA-3 (TWAJ), ROR-γt (BD2), Helios (22F6), IRF4 (3E4), Ki67 (SolA15), FcεR1a (MAR-1), CD11c (N418), CD4 (RM4-5), CXCR5 (SPRCl5), CD44 (IM7), CD62L (MEL-14), OX40 (OX86), GL-7 (GL-7), LAP (TW7-16B4), GARP (YGIC86), CD80 (16-10A1). CD25 (PC61.5), CD127 (A7R34), CD279 (J43) and cKit (2B8) were from eBiosciences. Anti-human mAb used in this study included CD3 (SK7), CD127 (A019D5), (Biolegend); CD4 (RPA-T4), LAP (TW4-6H10), FOXP3 (PCH101); CD25 (2A3), and ROR-γt (Q31-378) were from BD Biosciences; Cell viability dye (eFluor506) and (eF780) was from eBioscience. For cytokines cells were stimulated during 4 hours with PMA (50 ng/ml; Sigma-Aldrich) and ionomycin (500 ng/ml; Sigma-Aldrich) in the presence of Golgi Plug (BD Biosciences), then stained with the BD Cytofix/Cytoperm buffers (BD Biosciences) and the indicated anti-cytokine antibody. For intracellular staining of nuclear factors, the Foxp3 Transcription Factor buffer set (eBioscience) was used. Dead cells were routinely excluded from the analysis based on the staining of eFluor 506 fixable viability dye (eBioscience), and analyses were restricted to single cells using FSC-H and FSC-A signals. Stained cells were analyzed on an LSR Fortessa (BD Biosciences) and data were processed using Flowjo (Tree Star Inc.).

Quantitative real-time PCR for host immunological Targets

RNA was extracted from cells using RNeasy Mini kit (QIAGEN) according to the manufacturer protocol. Reverse transcription was performed with the SuperScript III RT-PCR system and random hexamer primers (Invitrogen) and quantitative real-time reverse transcription (RT)-PCR with Taqman® Fast Universal PCR master mix, internal housekeeping gene mouse (*Gapdh* FAM dye) and specific target gene primers for murine *Tgfb1, Tgfb2, and Tgfb3*, as indicated (FAM Dye) (Applied Biosystems) on Step-One-Plus machine. Relative expression was normalized to *Gapdh* and calculated as fold change compared to *Foxp3*^{YFPcre} Treg cells or Teff cells.

Bacterial consortia

The composition and preparation of the *Clostridiales* and *Proteobacteria* consortia has been previously detailed (Abdel-Gadir et al., 2019).

ELISA

Total, OVA-specific IgE and Murine mast cell protease 1 (MMCP-1) concentrations were measured in the sera of treated mice by ELISAs, as previously described (Abdel-Gadir et al., 2019).

TGF-β1 ELISA assays

$CD4^+$ T cells were enriched from mouse spleen by positive selection with anti-CD4 microbeads (Miltenyi Biotec). Enriched $CD4^+$ T cells were further purified with a cell sorter by gating on YFP^+CD4^+ T cells for Treg cells and YFP^-CD4^+ T cells for Teff cells. For monocyte purification, CD4 T cell-depleted splenocytes were stained with PE conjugated CD11b mAb, and the $CD11b^+$ cells were enriched by positive selection of anti-PE microbeads (Miltenyi Biotec). Monocytes were further purified from the enriched $CD11b^+$ cells with a cell sorter by gating on $CD11b^+Ly6C^+$ cells. B cells were sorted from CD4 and CD11b depleted splenocytes by gating on $CD19^+$ cells. Sorted cells were cultured at 0.5×10^6 cells/well (Treg and Teff cells) or at 1×10^6 cells/well (B cells and monocytes) in X-VIVO 15 media. $CD4^+$ T cells were activated in the presence of anti-CD3/CD28 dynabeads (Thermofisher) and 1 μg/ml of IL-2 (eBioscience) for 48h. B cells were activated with 10 μg/ml F(ab′)2 goat anti-mouse IgM antibodies (αIgM ; Jackson ImmunoResearch Laboratories) and 1 μg/ml recombinant CD40 ligand (CD40L; eBioscience) for 48h. Monocytes were activated with 1 μg/ml lipopolysaccharides (LPS; Sigma-Aldrich) for 48h. TGF-β1 cytokine amounts in the tissue-culture supernatant was detected using the TGF-β1 ELISA kit from R&D Systems (DY1679-05) according to the manufacturer's protocol.

Histology

Intestinal mast cells were counted by microscopic examination of jejunal sections fixed in 10% formaldehyde and stored in ethanol 70% before staining with toluidine blue by the Harvard Rodent Histopathology Facility.

Autoantibody array analysis

Autoantibody-by-autoantibody antibody analyses between group for differential expression were conducted using the R package 'limma' and multiple comparisons correction was performed in R (Ritchie et al., 2015). An antibody was considered statistically differentially antibody only if the Benjamini Hochberg-adjusted p value < 0.05 between the tested groups and the mean of expression of mutant group is 2-fold increase over wild group. The statistically significant autoantibodies were used to generated heatmap by heatmap.2 in gplots R package

B cell depletion

B cell depletion in 15 days old $Foxp3^{YFPcre}Tgfb1^{\Delta/\Delta}$ mice was performed by intraperitoneal injection of 200 μg anti-CD20 (clone AISB12, BioXCell) or IgG2a isotype control (clone 2A3, BioXCell) mAb per mouse weekly until the end of the survival analysis.

Mast cell suppression assay

Treg cells were purified from either $Foxp3^{YFPcre}$, $Foxp3^{YFPcre}Tgfb1^{\Delta/+}$ and $Foxp3^{YFPcre}Tgfb1^{\Delta/\Delta}$. Mast cells were differentiated from bone marrow as previously described (Burton et al., 2013). Mast cells and Treg cells were dispensed $5X10^4$ cells per well, respectively in conic 96 well plates, with 5ng/ml of IgE SPE7 (Sigma-Aldrich), 3ng/ml of mouse IL-3 (eBioscience), and CD3/CD28 activation beads were added accordingly to the manufacturer instructions (eBioscience), for a final volume of 100μl of RPMI. In some conditions mast cells were plated without Treg cells in the same final volume of 100μl of RPMI. After an overnight incubation at 37°, cells were stimulated for 10 min at 37°with DNP-BSA to assess the degranulation status of mast cells. 10μl of the 10x stimulus mix (500ng/ml DNP/BSA (sigma-Aldrich), 1/100 anti-LAMP-1 APC (Biolegend), 1/100 anti-ckit PE (eBioscience), 1/100 anti-CD4 FITC (Biolegend) and 1/1000 fixable viability dye eFluor 780 (eBioscience) were added per well. The reaction was stopped by adding 100μl/well of cold PBS/BSA containing 2mM EDTA. the plate was centrifuged for 3min at 1400rpm, the supernatants were discarded and the cells were suspended in 200μl/well of cold PBS/BSA and 2mM EDTA. The plate was centrifuged again for 3min at 1400rpm. The cells were suspended in 200μl of cold PBS/BSA and 2mM EDTA and the flow cytometry was performed immediately before losing the degranulation effect.

Treg cells adoptive transfer

$EGFP^+CD4^+DO11.10^+$ Treg cells were cell sorted from $Foxp3^{EGFPcre}$ and $Foxp3^{EGFPcre}Tgfb1^{\Delta/\Delta}$ mice, respectively. For treatment of established FA, $Il4ra^{F709}$ recipients were sensitized with OVA-SEB during 8 weeks. At week 9, the Treg-sensitized mice were given retro-orbitally at $5x10^5$ Treg cells of the respective genotype, sensitized with OVA-SEB for 4 more weeks and challenged at week 5 (150mg OVA). For FA prevention, $CD4^+$ $DO11.10^+Foxp3^{EGFP+}$ Treg cells were given retro-orbitally at $5x10^5$ cells/mouse on day 0 of the sensitization protocol. The mice were then sensitized with OVA-SEB for 8 weeks then challenged with OVA.

QUANTIFICATION AND STATISTICAL ANALYSIS

All experiments were performed using randomly assigned mice without investigator blinding. Results of Anaphylaxis temperature curves were analyzed by using 2-way ANOVA. Student's unpaired two tailed t test were used for 2 groups comparisons. For more than 2 groups, 1-way ANOVA with Tukey or Bonferroni post-test analysis using Prism 8 (GraphPad). Results are presented as means (horizontal lines or rectangular bars) and SEM where each point represents one sample. Differences in mean values were considered significant at a $p < 0.05$.

Immunity, Volume *53*

Supplemental Information

Regulatory T Cell-Derived TGF-β1 Controls Multiple Checkpoints Governing Allergy and Autoimmunity

Jacob A. Turner, Emmanuel Stephen-Victor, Sen Wang, Magali Noval Rivas, Azza Abdel-Gadir, Hani Harb, Ye Cui, Manoussa Fanny, Louis-Marie Charbonnier, Jason Jun Hung Fong, Mehdi Benamar, Leighanne Wang, Oliver T. Burton, Kushagra Bansal, Lynn Bry, Chengsong Zhu, Quan-Zhen Li, Rachel L. Clement, Hans C. Oettgen, Elena Crestani, Rima Rachid, Peter T. Sage, and Talal A. Chatila

Regulatory T cell-derived TGF-β1 Controls Multiple Checkpoints Governing Allergy and Autoimmunity

Jacob A. Turner[1,2*], Emmanuel Stephen-Victor[1,2*], Sen Wang[1,2], Magali Noval Rivas[3], Azza Abdel-Gadir[1,2], Hani Harb[1,2], Ye Cui[1,2], Manoussa Fanny[1,2], Louis-Marie Charbonnier[1,2], Jason Jun Hung Fong[1,2], Mehdi Benamar[1,2], Leighanne Wang[1,2], Oliver T. Burton[4], Kushagra Bansal[5], Lynn Bry[6], Chengsong Zhu[7], Quan-Zhen Li[7], Rachel L. Clement[8], Hans C. Oettgen[1,2], Elena Crestani[1,2], Rima Rachid[1,2], Peter T. Sage[8] and Talal Chatila[1,2,9 †]

[1]Division of Immunology, Boston Children's Hospital, Boston, MA, 02115 USA. [2]Department of Pediatrics, Harvard Medical School, Boston, MA, 02115 USA. [3]Division of Pediatric Infectious Diseases and Immunology, Department of Biomedical Sciences, Infectious and Immunologic Diseases Research Center (IIDRC), Cedars-Sinai Medical Center, Los Angeles, CA, 90048 USA. [4]Laboratory of Lymphocyte Signaling and Development, The Babraham Institute, Cambridgeshire CB22 3AT, UK. [5]Molecular Biology & Genetics Unit, Jawaharlal Nehru Centre for Advanced Scientific Research, Jakkur, Bangalore, 560064, India. [6]Massachusetts Host-Microbiome Center, Department of Pathology, Brigham & Women's Hospital, Harvard Medical School, Boston, MA, 02115 USA. [7]Department of Immunology and Internal Medicine, University of Texas Southwestern Medical Center, Dallas, Texas 75390, USA. [8]Transplantation Research Center, Renal Division, Brigham and Women's Hospital, Harvard Medical School, Boston, MA, 02115 USA

[9]Lead Contact

[*]These authors contributed equally to this work

†**Corresponding Author**. Email: talal.chatila@childrens.harvard.edu **(T.A.C).**

Fig. S1. Treg cell-specific overexpression of a *Tgfb1* transgene rescues FA. Related to Figure 1. (A) RT-PCR analysis of *Tgfb1* transcripts in sorted EGFP$^+$ and EGFP$^-$ CD4$^+$ T cells from MLN of *Foxp3*^{YFPcre}, *Foxp3*^{YFPcre}*Il4ra*^{F709} and *Foxp3*^{YFPcre}*Il4ra*^{F709}*Tgfb1*^{Tg} mice (8-12 weeks old). (B, C) LAP staining in Treg cells sorted from the MLN. (D) Changes in core body temperature in OVA-SEB-sensitized mice after oral OVA challenge. (E) Total and OVA-specific serum IgE and MMCP-1 concentrations before sensitization and after challenge. (F,G) Representative flow plots, frequencies and numbers of IL-4$^+$ and GATA-3$^+$ Treg and Teff cells from the MLN as determined by flow cytometry. Each symbol represents an independent sample. Numbers in flow plots indicate percentages. Error bars indicate SEM. Statistical tests: One-way ANOVA with Dunnett's post hoc analysis (A, E), two-way ANOVA (D); Student's *t*-test (C, G). *P<0.05, **P<0.01, ***P<0.001, ****P<0.0001. Data representative of two independent experiments. n=3-8 mice per group.

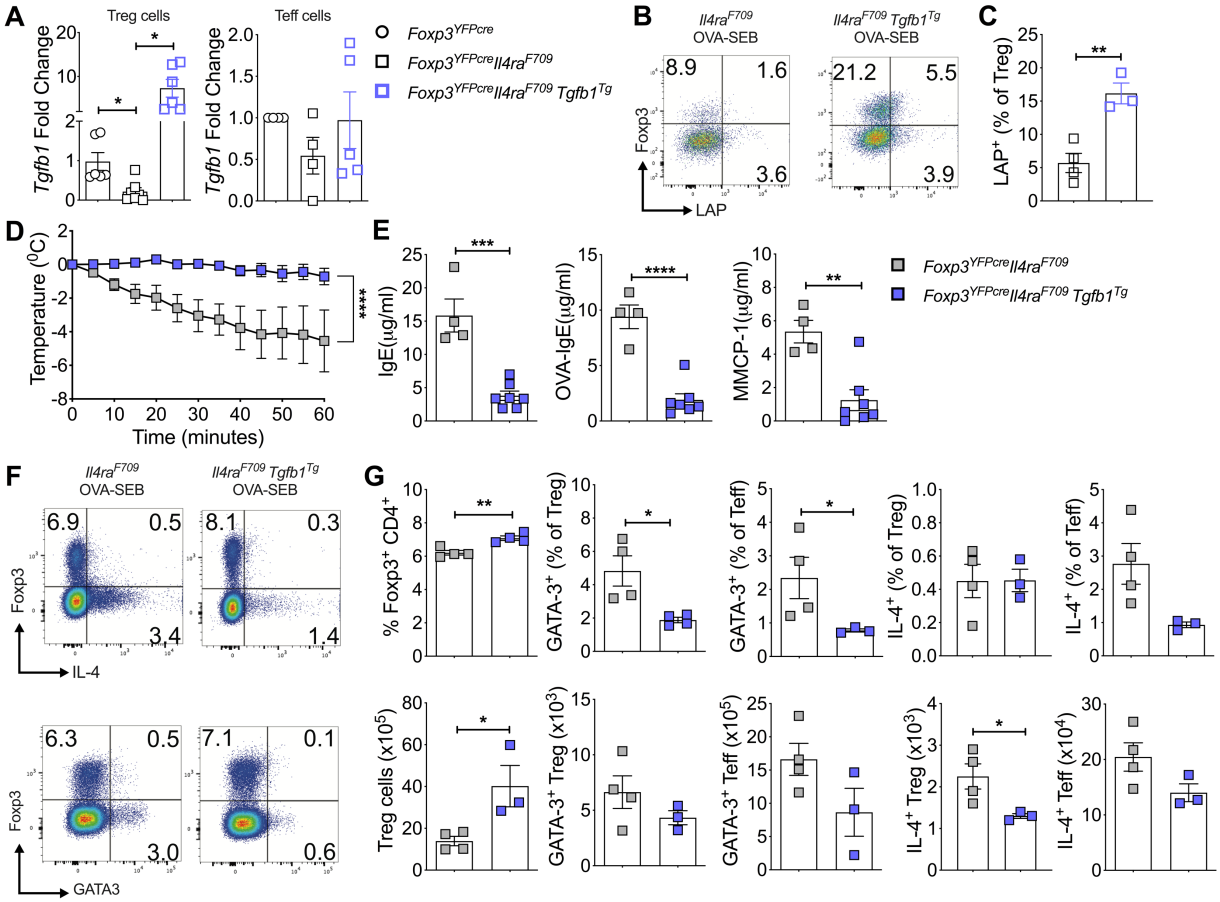
A
Treg cells
Teff cells
Tgfb1 Fold Change
Foxp3YFPcre
Foxp3YFPcreIl4raF709
Foxp3YFPcreIl4raF709 Tgfb1Tg
B
Il4raF709 OVA-SEB
Il4raF709 Tgfb1Tg OVA-SEB
8.9
1.6
3.6
21.2
5.5
3.9
Foxp3
LAP
C
LAP+ (% of Treg)
D
Temperature (0C)
Time (minutes)
E
IgE(μg/ml)
OVA-IgE(μg/ml)
MMCP-1(μg/ml)
F
Il4raF709 OVA-SEB
Il4raF709 Tgfb1Tg OVA-SEB
6.9
0.5
3.4
8.1
0.3
1.4
Foxp3
IL-4
6.3
0.5
3.0
7.1
0.1
0.6
GATA3
G
% Foxp3+ CD4+
GATA-3+ (% of Treg)
GATA-3+ (% of Teff)
IL-4+ (% of Treg)
IL-4+ (% of Teff)
Treg cells (x105)
GATA-3+ Treg (x103)
GATA-3+ Teff (x105)
IL-4+ Treg (x103)
IL-4+ Teff (x104)

Fig. S2. Characterization of TGF-β1 transcript and protein expression in immune cells of *Tgfb1* targeted mice. Related to Figure 6. (A) RT-PCR analysis of *Tgfb1* mRNA expression in Treg and Teff cells of littermate *Foxp3*^{YFPcre}, *Foxp3*^{YFPcre}*Tgfb1*$^{\Delta/+}$ and *Foxp3*^{YFPcre}*Tgfb1*$^{\Delta/\Delta}$ mice. (B and D) Flow cytometric analysis and frequencies of LAP^{+} (B) and GARP^{+} (D) cells from sorted Treg cells that were activated with 1μg/ml anti-CD3 mAb and 100U of IL-2 for 24h. (C) Frequencies of LAP^{+} Teff cells that were activated with 1μg/ml anti-CD3 mAb and 100U of IL-2 for 24h. (E to G) Quantification of TGF-β1 production by ELISA from FACS sorted Treg and Teff cells that were either sham treated or activated with anti-CD3+anti-CD28 mAb-coated dynabeads and 1μg/ml of IL-2 for 48h (E), from FACS sorted B cells that were either sham treated or activated with 10μg/ml αIgM and 1μg/ml recombinant CD40L for 48h (F), and from FACS sorted monocytes that were either sham treated or activated with 1μg/ml LPS for 48h (G). Each symbol represents an independent sample. Numbers in flow plots indicate percentages. Error bars indicate SEM. Statistical tests: One-way ANOVA with Dunnett's post hoc analysis (A to D), and Two-way ANOVA (E to G); **P<0.01, ***P<0.001, ****P<0.0001. Data representative of two independent experiments. n=4-14 mice per group.

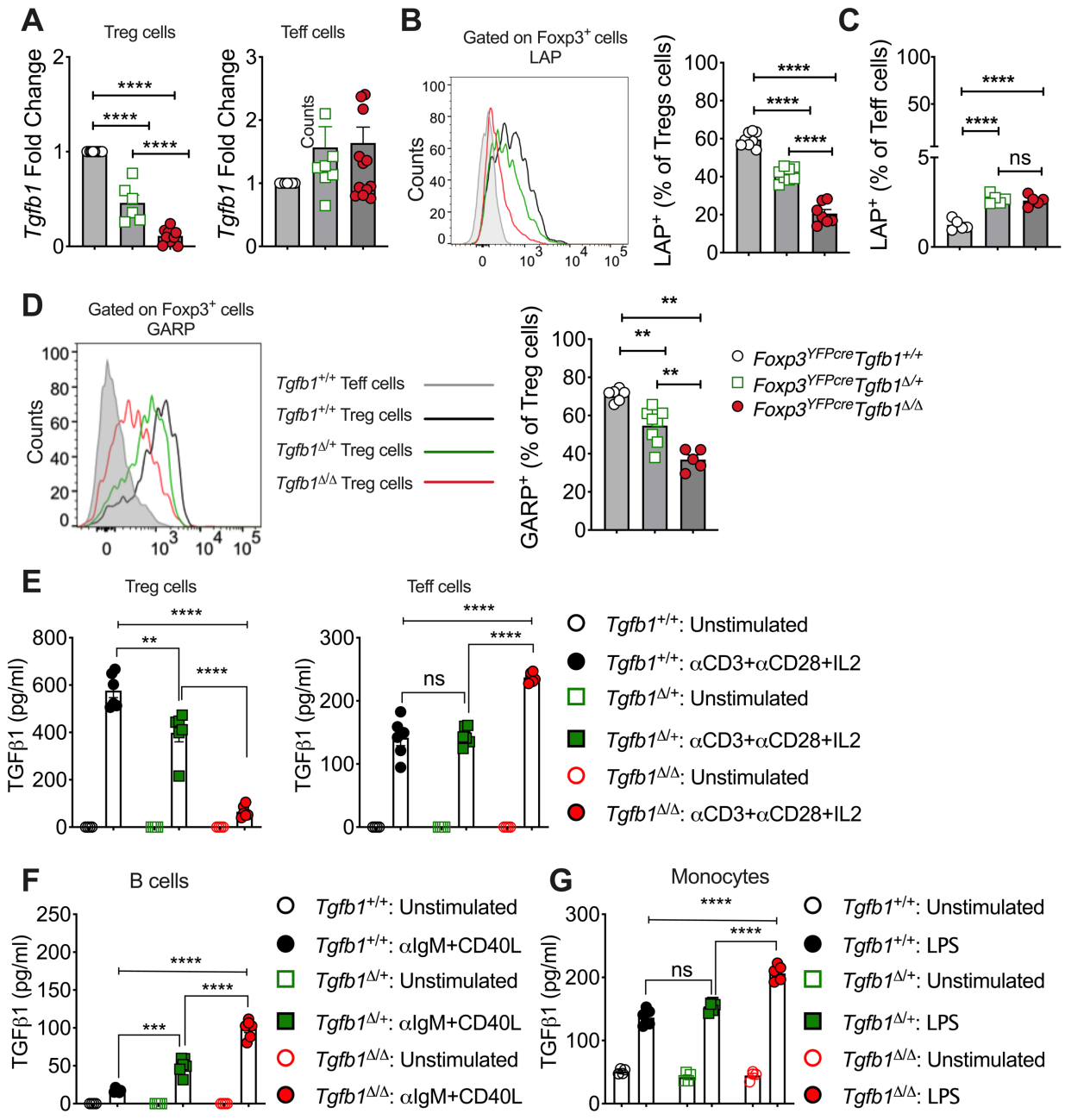
A
Treg cells
Teff cells
Tgfb1 Fold Change
Counts
B
Gated on Foxp3+ cells
LAP
Counts
LAP+ (% of Tregs cells)
C
LAP+ (% of Teff cells)
ns
D
Gated on Foxp3+ cells
GARP
Counts
Tgfb1+/+ Teff cells
Tgfb1+/+ Treg cells
Tgfb1Δ/+ Treg cells
Tgfb1Δ/Δ Treg cells
GARP+ (% of Treg cells)
Foxp3YFPcreTgfb1+/+
Foxp3YFPcreTgfb1Δ/+
Foxp3YFPcreTgfb1Δ/Δ
E
Treg cells
Teff cells
TGFβ1 (pg/ml)
ns
Tgfb1+/+: Unstimulated
Tgfb1+/+: αCD3+αCD28+IL2
Tgfb1Δ/+: Unstimulated
Tgfb1Δ/+: αCD3+αCD28+IL2
Tgfb1Δ/Δ: Unstimulated
Tgfb1Δ/Δ: αCD3+αCD28+IL2
F
B cells
TGFβ1 (pg/ml)
Tgfb1+/+: Unstimulated
Tgfb1+/+: αIgM+CD40L
Tgfb1Δ/+: Unstimulated
Tgfb1Δ/+: αIgM+CD40L
Tgfb1Δ/Δ: Unstimulated
Tgfb1Δ/Δ: αIgM+CD40L
G
Monocytes
TGFβ1 (pg/ml)
ns
Tgfb1+/+: Unstimulated
Tgfb1+/+: LPS
Tgfb1Δ/+: Unstimulated
Tgfb1Δ/+: LPS
Tgfb1Δ/Δ: Unstimulated
Tgfb1Δ/Δ: LPS

Fig. S3. Characterization of *Tgfb1*-deficient Treg cells. Related to Figure 6. (A) Flow cytometric analysis and MFI of CD25, CTLA4, OX40 and ICOS expression in splenic Treg cells. (B) Flow cytometric analysis and frequencies of Ki67 expression in $Foxp3^+$ and $Foxp3^-$ cells among splenic $CD4^+$ T cells. (C) Flow cytometric analysis and frequencies of IL-10 expression in $Foxp3^+$ and $Foxp3^-$ cells among MLN $CD4^+$ T cells. (D) Flow cytometric analysis and MFI of LAP in $CD11c^+MHCII^+$ DCs activated with 1μg/ml LPS for 24h (E) Flow cytometric analysis of an *in vitro* suppression assay with sorted $Foxp3^+$ cells from 8-12 weeks old $Foxp3^{YFPcre}$ (+/+), $Foxp3^{YFPcre}Tgfb1^{\Delta/+}$ (Δ/+), and $Foxp3^{EGFPcre}Tgfb1^{\Delta/\Delta}$ (Δ/Δ) Treg cells and cell-trace violet loaded WT Teff cells. (F) Flow Cytometric analysis of the frequency of YFP^+Foxp3^+ and YFP^-Foxp3^+ Treg cells in the spleen, MLN and LI-LP of female $Foxp3^{+/YFPcre}Tgfb1^{\Delta/\Delta}$. Each symbol represents an independent sample. Numbers in flow plots indicate percentages. Error bars indicate SEM. Statistical tests: Student's *t*-test (A and B), One-way ANOVA with Dunnett's post hoc analysis (C and D), and Two-way ANOVA (E); **P<0.01, ***P<0.001, ****P<0.0001. Data representative of two independent experiments. n=4-9 mice per group.

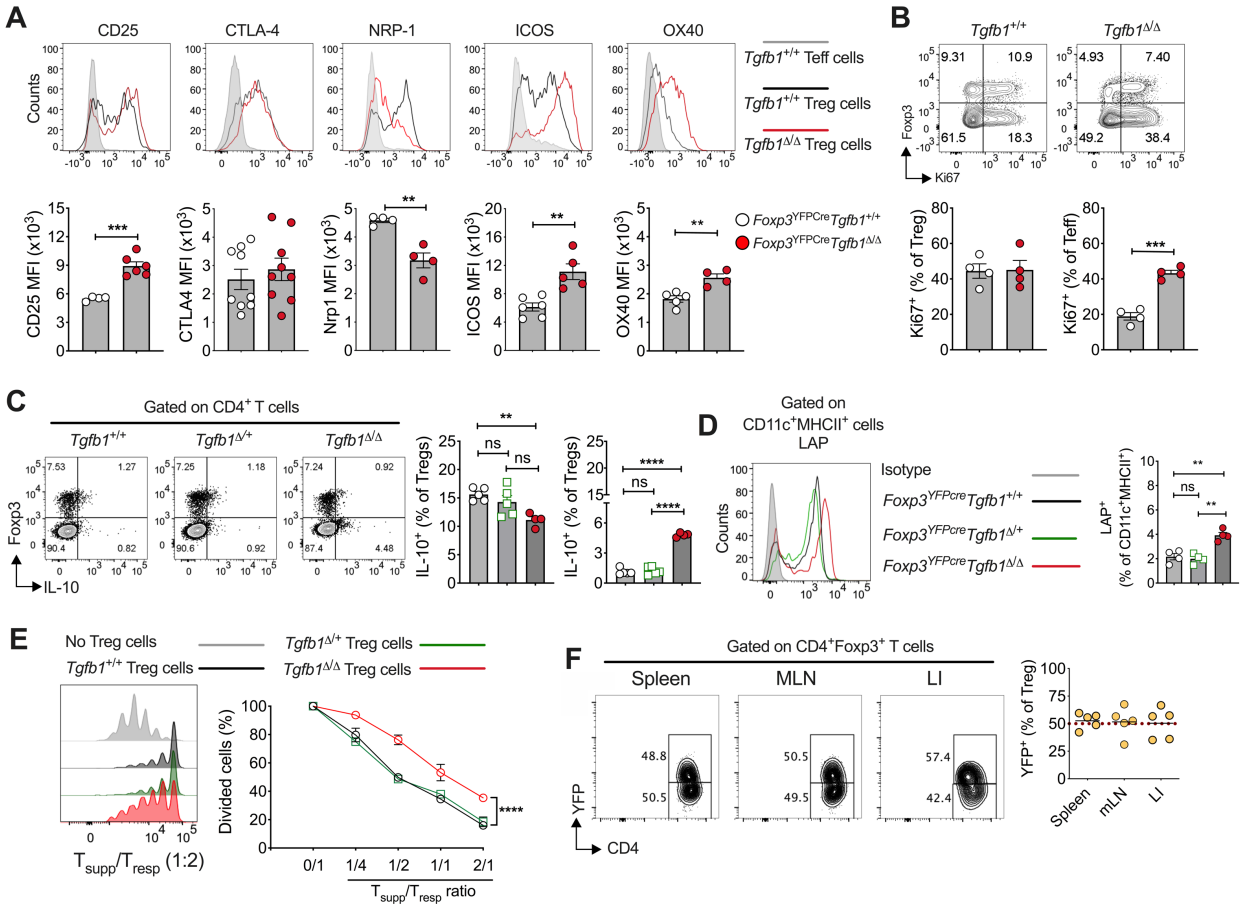
A
CD25
CTLA-4
NRP-1
ICOS
OX40
Counts
Tgfb1+/+ Teff cells
Tgfb1+/+ Treg cells
Tgfb1Δ/Δ Treg cells
CD25 MFI (x10³)
CTLA4 MFI (x10³)
Nrp1 MFI (x10³)
ICOS MFI (x10³)
OX40 MFI (x10³)
Foxp3YFPCreTgfb1+/+
Foxp3YFPCreTgfb1Δ/Δ
B
Tgfb1+/+
Tgfb1Δ/Δ
Foxp3
Ki67
9.31
10.9
61.5
18.3
4.93
7.40
49.2
38.4
Ki67+ (% of Treg)
Ki67+ (% of Teff)
C
Gated on CD4+ T cells
Tgfb1+/+
Tgfb1Δ/+
Tgfb1Δ/Δ
Foxp3
IL-10
7.53
1.27
90.4
0.82
7.25
1.18
90.6
0.92
7.24
0.92
87.4
4.48
IL-10+ (% of Tregs)
ns
D
Gated on CD11c+MHCII+ cells
LAP
Counts
Isotype
Foxp3YFPcreTgfb1+/+
Foxp3YFPcreTgfb1Δ/+
Foxp3YFPcreTgfb1Δ/Δ
LAP+ (% of CD11c+MHCII+)
E
No Treg cells
Tgfb1+/+ Treg cells
Tgfb1Δ/+ Treg cells
Tgfb1Δ/Δ Treg cells
Tsupp/Tresp (1:2)
Divided cells (%)
Tsupp/Tresp ratio
0/1
1/4
1/2
1/1
2/1
F
Gated on CD4+Foxp3+ T cells
Spleen
MLN
LI
48.8
50.5
50.5
49.5
57.4
42.4
YFP
CD4
YFP+ (% of Treg)

Fig. S4. Treg cell-specific *Tgfb1* deletion in *Foxp3*^{EGFPcre} mice is incompletely penetrant due to increased deletion escape. Related to Figure 6. (A) Representative flow cytometry plots acquired from the MLN of 8-12 weeks old *Foxp3*^{EGFcre}*R26*^{YFP} and *Foxp3*^{EGFPcre}*Tgfb1*$^{\Delta/\Delta}$*R26*^{YFP}. (Band C) Flow cytometric analysis and frequencies of LAP and GARP expression from EGFP^{+} and EGFP^{-} cells that were sorted from *Foxp3*^{EGFPcre}*Tgfb1*$^{\Delta/\Delta}$ and activated with 1μg/ml CD3 and 100U of IL2 for 24h. Expression of LAP (B) and GARP (C) in EGFP^{+} and EGFP^{-} cells stained for intracellular Foxp3 post activation. Each symbol represents an independent sample. Numbers in flow plots indicate percentages. Error bars indicate SEM. Statistical tests: Student's *t*-test (A***P<0.001. Data representative of two independent experiments. n=4 mice/group.

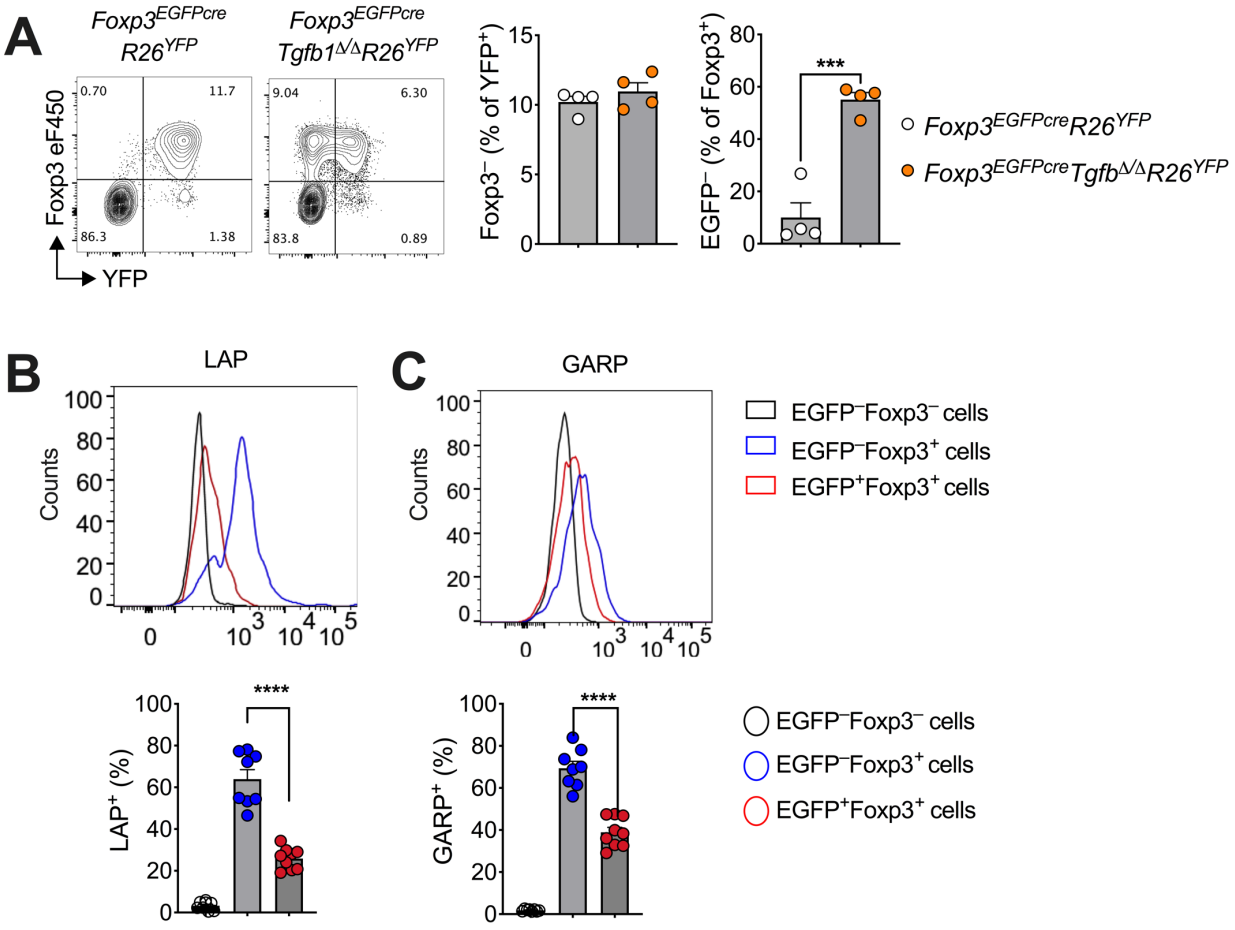

Fig. S5. Treg cell-specific *Tgfb1* deletion in *Foxp3*^{EGFPcre} mice promotes FA. Related to Figure 6. (A) Changes in core body temperature in OVA-SEB-sensitized WT, *Il4ra*^{F709} and *Foxp3*^{EGFPcre}*Tgfb1*$^{\Delta/\Delta}$ mice after 8 weeks of OVA-SEB sensitization followed by oral OVA challenge. (B) Total and OVA-specific serum IgE concentrations and serum MMCP-1 concentrations after anaphylaxis. (C) Representative histological sections from the SI-LP stained with Toluidine Blue. Magnified squares are 600x. (D) quantification the number of mast cells in the sections. (E to G) Flow cytometric analysis and frequencies and numbers of Foxp3$^+$ Treg cells (E), GATA-3$^+$ (F) and IRF-4$^+$ CD4$^+$ Treg cells (G) from the MLN. Each symbol represents an independent sample. Numbers in flow plots indicate percentages. Error bars indicate SEM. Statistical tests: One-way ANOVA with Dunnett's post hoc analysis (A, E), two-way ANOVA (D); Student's *t*-test (C, G). *P<0.05, **P<0.01, ***P<0.001, ****P<0.0001. Data representative of two independent experiments. n=9-18 mice per group.

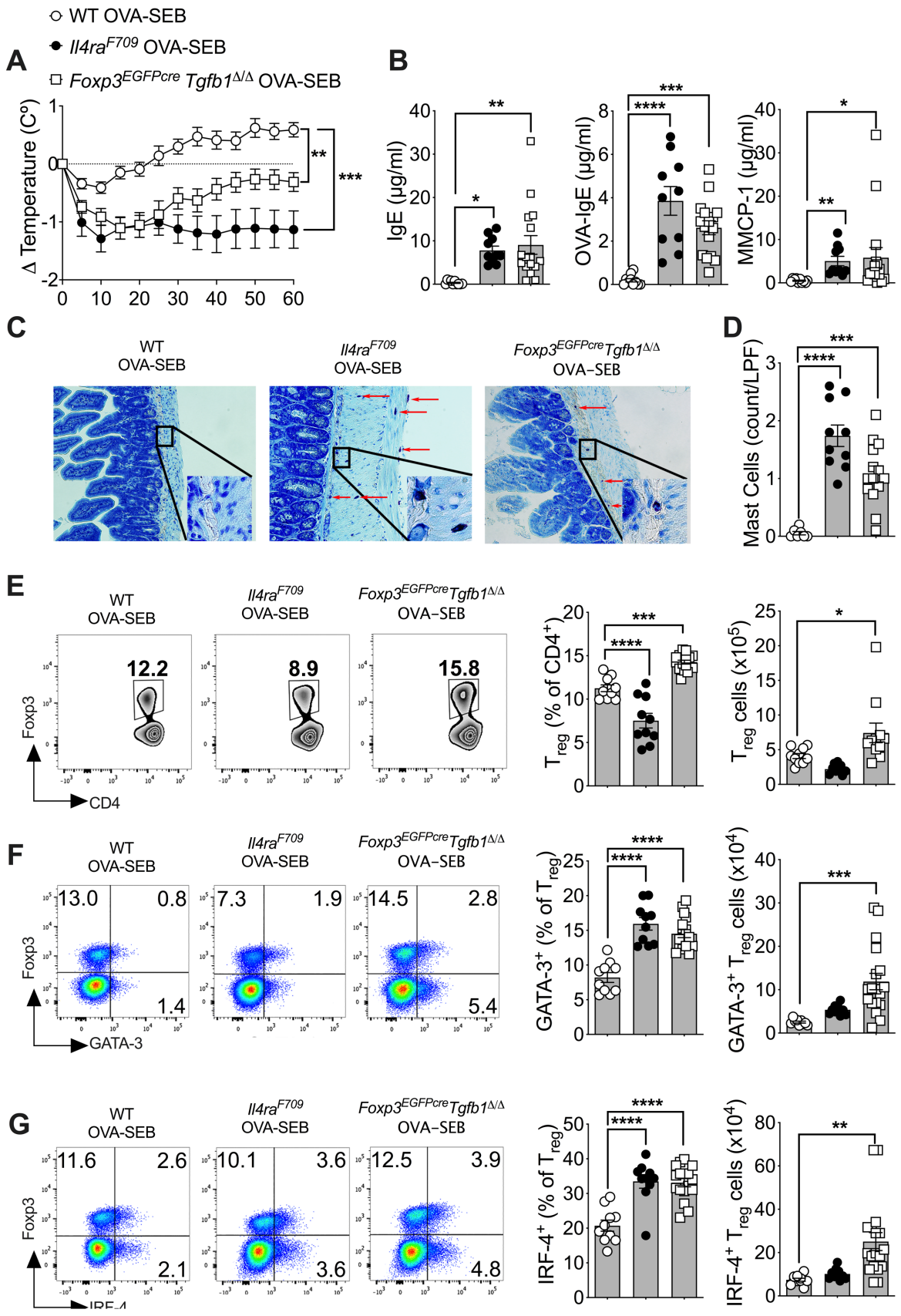
WT OVA-SEB
Il4ra^F709 OVA-SEB
Foxp3^EGFPcre Tgfb1^Δ/Δ OVA-SEB
A
Δ Temperature (C°)
B
IgE (μg/ml)
OVA-IgE (μg/ml)
MMCP-1 (μg/ml)
C
WT OVA-SEB
Il4ra^F709 OVA-SEB
Foxp3^EGFPcre Tgfb1^Δ/Δ OVA-SEB
D
Mast Cells (count/LPF)
E
12.2
8.9
15.8
Foxp3
CD4
T_reg (% of CD4+)
T_reg cells (x10^5)
F
13.0
0.8
1.4
7.3
1.9
14.5
2.8
5.4
GATA-3
GATA-3+ (% of T_reg)
GATA-3+ T_reg cells (x10^4)
G
11.6
2.6
2.1
10.1
3.6
3.6
12.5
3.9
4.8
IRF-4
IRF-4+ (% of T_reg)
IRF-4+ T_reg cells (x10^4)

Fig. S6. Adoptively transferred *Foxp3*^{EGFPcre}*Tgfb1*$^{\Delta/\Delta}$ Treg cells fail to prevent or rescue FA in *Il4ra*^{F709} mice. Related to Figure 6. (A to D) Preventative model. (A) Experimental scheme. CD4$^+$EGFP$^+$ Treg cells sorted from DO11.10$^+$*Foxp3*^{EGFPcre} (*Tgfb1*$^{+/+}$) and DO11.10$^+$*Foxp3*^{EGFPcre}*Tgfb1*$^{\Delta/\Delta}$ (*Tgfb1*$^{\Delta/\Delta}$) mice were transferred into *Il4ra*^{F709} mice, which received 8 weeks of OVA-SEB sensitization and were then orally challenged with OVA. (B) Core body temperature changes after oral OVA challenge. (C) Total and OVA-specific serum IgE and serum MMCP-1 concentrations after anaphylaxis. (D). Frequency of IL-4$^+$ and GATA-3$^+$ CD4$^+$ T cells from the MLN as determined by Flow Cytometry. (E to H) Curative model. (E) Experimental scheme. CD4$^+$EGFP$^+$ Treg cells derived as in (A) were transferred into OVA-SEB-sensitized *Il4ra*^{F709} mice, which were further sensitized for four weeks then challenged with OVA. (F) Core body temperature changes after oral OVA challenge. (G) Total and OVA-specific serum IgE and serum MMCP-1 concentrations. (H). Frequency of IL-4$^+$ and GATA-3$^+$ CD4$^+$ T cells from the MLN. Each symbol represents an independent sample. Numbers in flow plots indicate percentages. Error bars indicate SEM. Statistical tests: two-way ANOVA (B,F); Student's *t*-test (C, D, G, H). *P<0.05, **P<0.01, ****P<0.0001. Data representative of two independent experiments. n=5-8 mice per group.

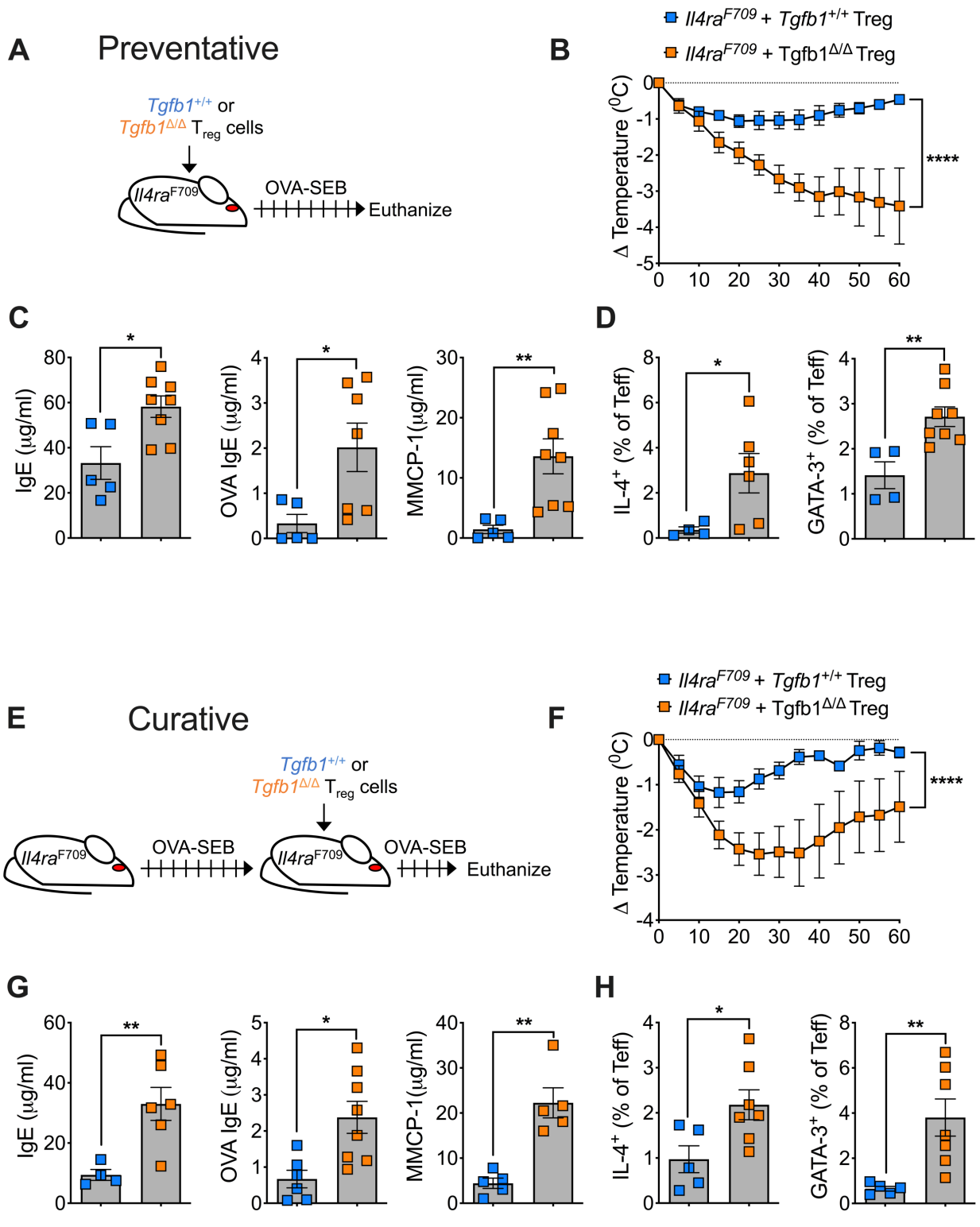
A
Preventative
Tgfb1+/+ or
Tgfb1Δ/Δ Treg cells
Il4raF709
OVA-SEB
Euthanize
B
Il4raF709 + Tgfb1+/+ Treg
Il4raF709 + Tgfb1Δ/Δ Treg
Δ Temperature (0C)
****
C
IgE (μg/ml)
OVA IgE (μg/ml)
MMCP-1(μg/ml)
D
IL-4+ (% of Teff)
GATA-3+ (% of Teff)
E
Curative
F
G
H

Fig. S7. Humoral autoimmunity in *Foxp3*^{YFPCre}*Tgfb1*$^{\Delta/\Delta}$ mice. Related to Figure 7. (A to C) Heat map representation of serum IgM (A), IgA (B) and IgE (C) autoantibodies in *Foxp3*^{YFPcre}, *Foxp3*^{YFPcre}*Tgfb1*$^{\Delta/+}$, and *Foxp3*^{YFPcre}*Tgfb1*$^{\Delta/\Delta}$ littermate mice. Each column number represents an independent mouse. Statistical tests: R package 'limma' and multiple comparisons corrections adjusted to $p<0.05$ (A to C). Data representative of at least two independent experiments with 5 mice per group.

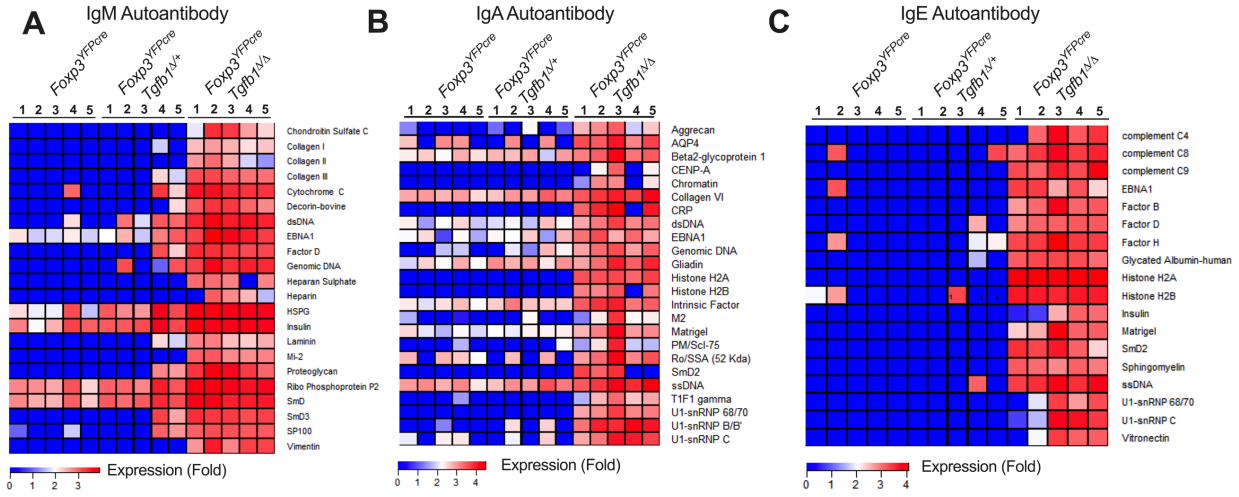

Table S1. Demographic characteristics of Study Subjects. Related to Figure 1.

	Gender	Age (years)	Phenotype
Healthy Controls	F	6	HC
	F	7	HC
	F	8	HC
	M	2	HC
	M	11	HC
	F	6	HC
Atopic Controls	M	4	AD
	M	17	AR
	F	4	AR, AD
	F	1	AD
	M	12	AS, AR
	F	14	AS, AR
	F	19	AR
	M	7	AS, AR
	M	20	AS, AR, AD
	F	8	AR, AD
	M	14	AS, AR
	M	12	AS, AD
	M	14	AS, AD
	M	7	AS
	M	10	AS
	M	11	AR, AD
	M	9	AR
	M	10	AR
	M	12	AS
	F	8	AS, AR, AD
	F	17	AS, AR
	M	14	AS, AR, AD
	M	15	AS, AR
	M	9	AS, AR
Food Allergic Subjects	M	14	FA (peanut, milk, tree nuts, seafood), AS, AR
	M	14	FA (peanut, tree nuts), AS, AR
	M	5	FA (peanut, tree nuts, egg, shellfish), AS, AR, AD
	F	10	FA (peanut, tree nuts, egg, salmon, trout, anchovy)

	F	2	FA (peanut, wheat, barley, rye, oat, almond), AS, AR, AD
	M	1	FA (peanut, milk, soy, egg, wheat, tree nuts, sesame), AD
	M	13	FA (peanut, egg)
	M	14	FA (peanut, tree nuts), AS, AR
	M	1	FA (peanut, tree nuts)
	F	15	FA (peanut, tree nuts, egg, shellfish, lentils, peas, sesame, chickpeas), AS, AR
	F	2	FA (peanut, milk, egg, soy, tree nuts), AD
	F	11	FA (peanut, tree nuts), AR, AD
	F	3	FA (peanut, tree nuts, soy, sesame, sunflower seed, poppy seed, chickpea, lentil, lima bean, fish, shellfish), AR, AD
	F	7	FA (egg, milk, tree nuts)
	M	14	FA (peanut, egg, tree nuts, fish, shellfish), AS, AR
	M	5	FA (egg), AR
	F	17	FA (avocado), AR, AD
	F	3	FA (peanut, tree nuts), AD
	M	7	FA (peanut, tree nuts, egg), AS, AR
	F	10	FA (peanut), AS, AR
	M	11	FA (peanut, tree nuts)

HC: healthy control; FA: food allergy; AS: asthma; AR: allergic rhinitis; AD: atopic dermatitis